COO-1198-1277

MASTER

DEPARTMENT OF CERAMIC ENGINEERING

UNIVERSITY OF ILLINOIS

URBANA, ILLINOIS

DISCLAIMER

HYDROGEN CHEMISORPTION AND OXIDATION ON TRANSITION METAL CARBIDES

BY

JAMES ROGER BETHIN

B.S., University of Rochester, 1972
M.S., University of Illinois, 1974

THESIS

Submitted in partial fulfillment of the requirements for the degree of Doctor of Philosophy in Ceramic Engineering in the Graduate College of the University of Illinois at Urbana-Champaign, 1979

Urbana, Illinois

HYDROGEN CHEMISORPTION AND OXIDATION ON TRANSITION METAL CARBIDES

James Roger Bethin, Ph.D.
Department of Ceramic Engineering
University of Illinois at Urbana-Champaign, 1979

This work has been a study of the catalytic activity of tungsten carbide, focusing on the possible influence of point defects.

The chemisorption of hydrogen on tungsten carbide and titanium oxycarbides was studied with differential scanning calorimetry. The catalytic activity of these materials for oxidation of hydrogen was determined by potentiostatic steady-state and potentiodynamic measurements in acid electrolye. Compositions of tungsten carbide surfaces were determined by X-ray photoemission and related to the catalytic behavior. Titanium oxycarbide surfaces were analyzed by Auger electron spectroscopy.

Of the carbides tested only one WC preparation was able to chemisorb hydrogen. Both WC powders investigated catalyzed hydrogen oxidation with similar specific activities.

Spectroscopic studies showed that the active surface of tungsten carbide was a mixture of WO_3 and a carbon-deficient WC phase. This result indicates that carbon vacancies are the active sites in tungsten carbide. Theoretical models of a carbon vacancy surrounded by metal atoms suggested by calculations by other workers support this assignment and identify the

important role of the W6s level. The measured value of the heat of chemisorption is consistent with the proposed model.

ACKNOWLEDGEMENTS

The author would like to gratefully acknowledge the support given him by his advisor Dr. Wendell S. Williams. He would also like to thank the other members of his research group for their cooperation and help: D. Gross, C. Maurer, N. K. Sharma, and L. Dy.

The author is most grateful to his typist, Chris Walling, whose endurance and intelligence made this work much easier to complete.

This work was supported through the Materials Research Laboratory by the Department of Energy under Contract. DOE EY-76-C-02-1198.

TABLE OF CONTENTS

CHAPTER 1

I. INTRODUCTION

A. Background

In the past several years heterogeneous catalysis has received much attention because of its great technological importance and because advances in the spectroscopy of solid surfaces and in the development of powerful computational methods have made recent investigations much more productive. Heterogeneous catalysis is, in practice, the process in which the presence of a solid surface enhances the rate of reaction between liquid or gas reactants. Typically, this involves adsorption of at least one reactant onto the catalyst surface, formation of a temporary intermediate product on the surface, and desorption of the final products into solution or gas phase. To understand catalytic mechanisms, it is necessary to investigate the nature and position of the chemisorption bond and the subsequent surface processes. Much of the present thinking concerning heterogeneous catalysis is dominated by the concepts of unsaturated coordination and the local site. Recent work on ceramic materials has made it clear that catalytically active sites on the surface are often associated with point defects such as vacancies.

Tungsten carbide has the remarkable property [1] of being able to react oxygen and hydrogen together at room temperature to form water, something which obviously does not occur at any measurable rate in the gas phase, and which previously was only known to take place on platinum-group metals. This platinum-like catalytic activity of tungsten carbide is also found for several other reactions. The scientific objective of the present study is to explain the platinum-like catalytic behavior of tungsten carbide in terms of its electronic, crystallographic, and defect structure; the technological objective is to suggest alternative

electrode materials for use in acid fuel cells. In this study the electrocatalytic oxidation of hydrogen and the chemisorption of hydrogen on tungsten carbide and titanium oxycarbide was investigated.

Hydrogen oxidation on the transition metal carbides is an attractive system for the study of catalysis, both from the point of view of simplicity and from that of its technological application as the anodic reaction in the hydrogen-oxygen fuel cell. The overall reaction is for the H_2 molecule to form two H^+ ions in the acid electrolyte, leaving two electrons in the carbide electrode. On tungsten carbide this is a two-step process:

$$H_2 \rightarrow 2H(ads) \rightleftarrows 2H^+(solution) + 2e^-(carbide).$$

The first step, which is the important rate-limiting step, [2,3] is the dissociative chemisorption of H_2 on the carbide surface to give adsorbed H atoms. In the gas phase, this step is a simple molecular process which can be separately studied and modeled theoretically.

B. Adsorption Phenomena

A variety of events may occur when a molecule comes into contact with a solid surface. It may be reflected with no energy loss or it may lose only a small amount of energy and be inelastically reflected. On the other hand, and importantly for catalysis, the molecule may give up enough energy to the surface that the new molecule-surface system is stable with the molecule adsorbed or bound to the surface. For catalysis, adsorption of reactants can hasten the reaction toward equilibrium by concentrating the reactants at the surface, by lowering the reaction activation energy, and by possibly hindering competing reactions.[4]

Physical adsorption (or "physisorption") is the weak bonding resulting from van der Waals forces. This is shown by the curve

$2M + H_2$ in Figure 1. E_p represents the energy of physical adsorption of an H_2 molecule and is typically 5.8 kcal/mole (0.25 eV) or less. Physisorption is non-selective with regard to the surface. The adsorbate may, in fact, condense to form a multi-layer interface. As with simple evaporation, E_p may be overcome by prolonged evacuation at or below the boiling point of the adsorbate. Since great specificity is observed when a given reaction is catalyzed by different surfaces, physisorption cannot itself be responsible for the acceleration of a reaction by a catalyst.

It is more usual for some degree of electron transfer or sharing to occur between the molecule and the surface. In this case the physisorbed molecule undergoes vibrational or electronic excitations which may allow it to overcome an activation energy equal to $E_c + E_p$ in Fig. 1, whereupon the molecule finds itself strongly chemically adsorbed (or "chemisorbed") with an energy E_a to surface atoms. In the case of the hydrogen molecule the activation energy needed involves dissociation of the molecule into atoms while it is being chemically bound to the surface. A typical value of E_a on a good chemisorber is 35 kcal/mole for H_2 on polycrystalline tungsten. As an energetic condition for H_2 chemisorption from Fig. 1 we find:

$$E_a = 2E_b - D_{H_2} > E_p \quad , \qquad (1)$$

or E_b must be greater than about 54 kcal/mole, although there may still be a consequential activation energy to adsorption.

A general observation can be made relating the strength and rate of chemisorption of reactants onto a catalyst to activity of the catalyst for the overall reaction. Maximum activity results when the chemisorption of the reactants is fast but not so strong that the reactants cannot be released for completion of the reaction. Optimum activity corresponds to intermediate coverage of the chemisorbed reactant over the catalyst surface.

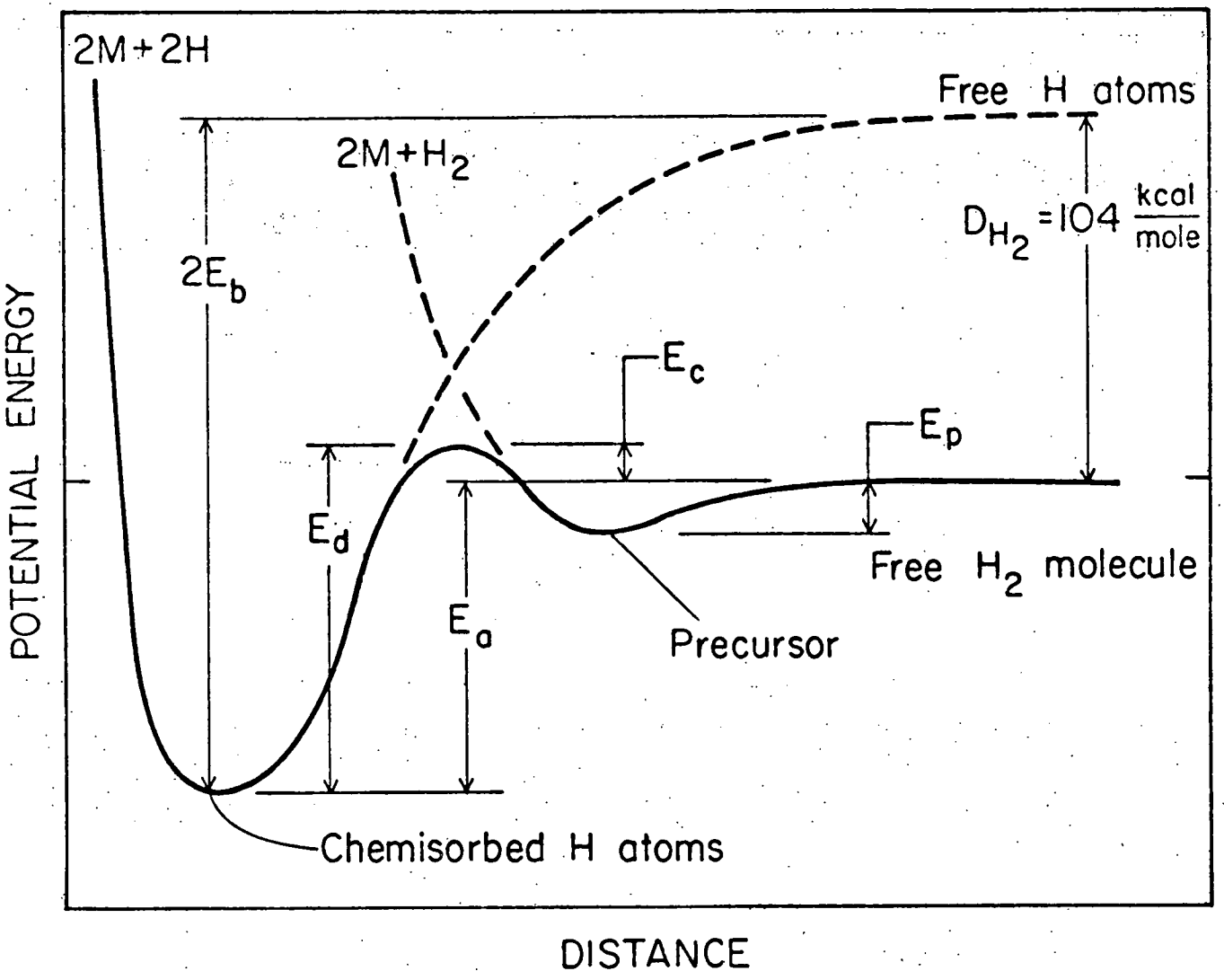

Figure 1. Dissociative adsorption of molecular hydrogen on a surface.

Trasatti [5] illustrates this nicely for electrolytic hydrogen evolution on the sp and transition metals with what is now commonly called a "volcano" curve. By plotting essentially the electrocatalytic activity for hydrogen evolution versus M-H bond strengths an impressive maximum in the electrocatalytic activity was found for intermediate coverages of hydrogen and intermediate bond strengths, with platinum having the best compromise of chemisorptive properties. Trasatti also notes that as we move down the volcano curve on the high M-H bond strength side it is likely that the reaction will change which step is rate determining or may change reaction path altogether as the stability of the M-H bond more severely limits the reaction rate.

C. Previous Carbide Catalytic Studies

Platinum has in the past been the most satisfactory catalyst in many reactions, e.g., for hydrogen oxidation in fuel cells. However, platinum is expensive and more importantly, it is severely poisoned by the hydrogen sulfide and carbon monoxide present in reformed hydrogen fuels. The stimulus for most of the past work on tungsten carbide as a catalyst was the idea that it might avoid some of the problems of platinum as the anode material. Tungsten carbide is a lower-cost, corrosion-resistant material and has been found to possess activity for hydrogen oxidation approaching that of platinum [2,6-8] and has the same two-step reaction for hydrogen oxidation: $H_2 \rightarrow 2H_{ads} \rightarrow 2H^+ + 2e^-$, with the first step, the Tafel reaction, being rate determining. [2,3] Tungsten carbide is not poisoned at any level of carbon monoxide, nor by several V.ppm hydrogen sulfide. [9-11] After these promising preliminary investigations, groups in Germany, [12-14] Czechoslovakia, [15] the Soviet Union, [16], England, [17], and the United States, [18,19] have worked toward the development of tungsten carbide as a fuel cell catalyst. Progress has been made, but results are sometimes conflicting and a good understanding of the high activity of tungsten carbide is lacking.

The earliest efforts to understand the activity of tungsten carbide attempted to correlate activity with electronic distribution for tungsten and molybdenum, their carbides, and platinum. Levy and Boudart [1] reported that tungsten carbide exhibited platinum-like behavior for several gas-phase reactions and does in fact chemisorb hydrogen. They speculated that the change in electron distribution in tungsten by addition of carbon tames the much too high reactivity of tungsten with oxygen by the shift of the carbon valence electrons to the metal. Using X-ray photoemission spectroscopy (XPS), Bennett, et al., [20] showed that the density of states at the Fermi level, $N(\varepsilon_f)$, for tungsten carbide more nearly resembles that of platinum than that of tungsten. They suggested that a high $N(\varepsilon_f)$ is necessary, although not sufficient, for high catalytic activity. Colton, et al., [21] agreed with this in their XPS measurements, but found that the electron density shifts from tungsten 5d to carbon 2p levels. This result suggests that bulk electronic properties are unable to adequately explain the catalytic activity of tungsten carbide.

The electrocatalytic activity of tungsten carbide has been shown in numerous studies to depend greatly on the method of preparation [8,9,15] aside from surface area differences. It has also been reported that the activity of tungsten carbide can be increased by various activation schemes, [13,22] and carbides with a bulk deficiency of carbon are thought to be more active than stoichiometric forms. [13,15] Ross and Stonehart [19] examined various tungsten carbide preparations with Auger Electron Spectroscopy (AES) to determine surface compositions and with XPS to determine chemical states of atoms at the surface. These factors were related to the electrocatalytic activity of the carbide for hydrogen oxidation in acid. The more active compositions were found to have several common characteristics: (1) no surface layer of free carbon, (2) surface tungsten atoms were a mixture of oxidized and carbidic tungsten ions, and (3) oxygen was present on the surface. The most active composition was a

carbon deficient preparation with significant amounts of oxygen in the bulk. An oxidation treatment at 350°C for 30 minutes deactivated stoichiometric tungsten carbide and oxidized it into the bulk. Sub-stoichiometric tungsten carbide was activated and surface free carbon was removed without substantial oxidation into the bulk. Rose and Stonehart conclude that since tungsten chemisorbs and dissociates hydrogen molecules in the gas phase, it is the function of the carbon atoms in the carbide to reduce the interaction of the tungsten ions with oxygen and water. They suggest that the oxygen in the carbide is substituted into the lattice for carbon and further stabilizes both the tungsten and carbon to oxidation. They conclude that O-W-C sites are able to adsorb H_2 due to reduced attack from the H_2O molecules in the electrolyte.

On the other hand, Palanker, et al., [16] recently measured the electrocatalytic activity of both high and low surface area WC powder with different carbon proportions and contend that correction of the activity for the surface area of the powders removed the differences in activity. They found that electrochemical anodic activation of the carbide catalyst oxidized the surface according to X-ray diffraction patterns and they believe that the effect of this was to simultaneously decrease the particle size and thus increase the surface area, which explains the increased activity.

Other carbides have been examined also. Mo_2C was found to catalyze ethane hydrogenolysis.[23] Stoichiometric TiC was shown not to catalyze hydrogen oxidation [7,24] and a surface film, perhaps TiO_{2-x} was formed. Goretzki and coworkers [25] found carbon deficient TiC adsorbs hydrogen at elevated temperatures. Hydrogen adsorption and hydrogen oxidation were found for W_2C at levels below that on WC. [18] Thus, although the problem of catalysis by transition metal carbides has been investigated in several laboratories, the actual atomic environment on the surface responsible for the hydrogen molecule adsorption is still in dispute.

D. Theoretical Considerations

In the previous discussion of chemisorption it was implied that the chemisorption bond is localized at a surface site. This is supported by much of the recent heterogeneous catalysis work. On metals these highly active sites might be nearly singly dispersed metal atoms supported on a stable substrate or corner or edge metal atoms on a powder or single crystal. [26] For non-metals [27,28] these active sites are usually present in low concentrations on the surface and are often associated with point defects and ions of unsaturated coordination or unusual charge states.

The question of chemisorption and the influence of surface defects on chemisorption can be approached through cluster calculations. For these calculations the chemisorption site to be investigated is modeled with a small cluster of surface atoms and an adsorbate atom. Various methods can be used with high speed digital computers to produce M-H potential energy curves (see curve 2M-2H in Fig. 1), the binding energy, and several other chemisorption parameters. Using first-principle methods, such as Hartree-Fock, Kunz and coworkers [29,31,32] have made several unexpected and important discoveries of chemisorption behavior which will be seen to provide valuable models for this experimental study.

Work on nickel metal and other first period transition metals by Kunz and coworkers [29] indicates a largely s or sp hybrid character to the M-H chemisorption bond. They find that a Ni atom bound to a substrate will have the $3d^9 4s$ configuration. As the hydrogen atom approaches, it begins to bond with the singly occupied 3d orbital and is weakly attracted to the surface. As the hydrogen atom moves closer to the surface, the $3d^8 4s^2$ state becomes dominant when the hydrogen atom is bound, so that the hydrogen bonds with a 4s or 4sp orbital, instead of following the conventional classical assumption of bonding with the d hole

or unfilled d shell. Attempts to correlate catalytic activity of transition metals with d-character are common, but recent reviews by Sinfelt [4] and by Madey, et al., [28] have expressed reservations about the adequacy of the d-bonding correlation, especially when comparing different transition metal periods. This study could answer those reservations. One cautionary note should be injected here. The same experiment (Demuth [30]) that confirms the sp character of the Ni-H chemisorption bond also shows that there is strong d-bonding for H on Pd or Pt in the next two transition metal series. Therefore the conclusions from the study of H on Ni may not apply to all other systems.

In parallel studies H atom adsorption on NiO [31] and CaO [32] (100) surfaces were investigated by cluster calculations. Both the empty Ni4s and, again, the unfilled Ni3d remain inert, as the H adsorbs only weakly to the perfect NiO surface. If a Ni^{2+} ion vacancy is created, however, as is common in the real material, an O^{2-} ion converts to an O^{-} ion, which forms a strong bond with the H. Klein [32] has shown the similarity of this bond to the familiar covalent bond in the $(OH)^{-}$ molecule. The perfect surfaces of these materials are essentially inert, but a metal ion vacancy on the surface allows an O^{-} ion to form, which provides the active site in these materials. This result is contrary to the classical argument that the metal d-electrons are the primary factor in the chemisorption process. [33]

The usefulness of these models is demonstrated with regard to titanium carbide, TiC. Jennison, et al., [34] have done an unrestricted Hartree-Fock calculation of a TiC_5 cluster to simulate the (100) surface. Overlap with the C2s pushes the Ti4s state up 7.8 eV above the $3d^3$ level, draining the electrons out of the 4s state. This leaves only a dangling 3d orbital at the surface. From the work of Kunz, et al., above it can be predicted that hydrogen will not bind to the perfect TiC surface.

Klein [32] has performed the H-TiC_5 calculation and found essentially no chemisorptive bond. This agrees with previously cited work [7,24] which shows no chemisorption of hydrogen on stoichiometric TiC. Two predictions, however, can be made for non-stoichiometric TiC_x from these cluster models. Although the 4s band in $TiC_{1.0}$ is energetically out of reach for use in bonding to hydrogen, TiC_x may present an intermediate case, where the Ti4s comes down far enough to form a $4s^1 3d^{n-1}$ configuration which will be more favorable to hydrogen chemisorption. This appears to be corroborated by the fact that TiC_xH_y does form from the substoichiometric carbide. A second prediction was made by Klein, [32] who suggests that the active site on TiC is an oxygen atom substituting for a surface carbon ion. The oxygen atom is predicted from the Madelung constants to be the O^- state. From the previous arguments the oxygen point defect can be predicted to be active for molecular hydrogen chemisorption on TiC_x. An inverse cluster calculation with a carbon vacancy, i.e., $\square C_5$, has not yet been done.

A similar analysis can be applied to tungsten carbide, where Ross and Stonehart [19] found the catalytically-active samples to be significantly carbon deficient and to contain oxygen on the surface. However, the author feels this analogy must be made with some caution.

The radial extent and the polarizability of the W5d states are much larger than those of the 3d orbitals in the first transition metal series, and may be involved to some degree in hydrogen chemisorption and oxidation. However, the variability of the activity of tungsten carbide with preparation, that is, with oxygen and carbon content, suggests contributions from these same models: that is, 6s involvement as the carbon content decreases, and O^- active sites for hydrogen chemisorption.

E. Design of Present Study

In view of the above models it was believed that investigating chemisorption and electrocatalytic oxidation of hydrogen on the TiC_xO_y system could test both the role of O^- in carbide catalysis and that of the s orbital. In addition, samples of WC believed to be of distinctly different bulk and surface composition were examined with the idea of interpretation in terms of these models and the results found from the TiC_xO_y system. The following chapter will describe the use of various techniques to study these powders. Pressure Differential Scanning Calorimetry was used to investigate heats of chemisorption of hydrogen on the carbide powders. Auger electron spectroscopy and X-ray photoelectron spectroscopy were used to characterize surface composition and chemical states of ions at the surface. Potentiodynamic and potentiostatic electrochemical measurements were made to examine the electrocatalytic activity of the carbides for hydrogen oxidation. In addition, various ancillary techniques are also described with respect to their use with the materials of this study. The results support the participation of carbon vacancies in hydrogen chemisorption on carbides and add more weight to the general idea that chemisorption and heterogeneous catalysis often involve point defects in solids.

CHAPTER 2

EXPERIMENTAL APPARATUS AND PROCEDURES

A. Starting Materials

Titanium carbide powders used in this study were from several sources. Powders of adequate purity (greater than 99.8 atomic % excluding oxygen and at least -400 mesh are generally not offered commercially at this time, due largely to their extreme hardness and resistance to grinding. One powder was obtained from Cerac, Inc., and use was made of a small stock in our laboratory of high purity titanium carbide powders. Chemical analyses of the powders are shown in Table 1. The results were obtained using spark-source mass spectrography. $TiC_{.940}$ was a ground single crystal while all other powders were formed by high temperature reaction of the elements. Ultra Superior Purity Carbon Powder from Ultra Carbon Corp. with no detectable impurities and titanium monoxide powder from Cerac, Inc. were used to prepare powders in the system TiC_xO_y. No additional detectable impurities were introduced in the preparation process.

The tungsten carbide powders were from three sources. A sample of the tungsten carbide labeled WC 165 in the work of Ross and Stonehart [19] was obtained from Dr. P. N. Ross, Jr., at United Technologies Corporation. This material was prepared by carburization of the white (amorphous) modification of tungstic acid. The white (amorphous) tungstic acid was mixed with 10 w/o NH_4Cl and carburized at 900°C for 2 hrs in flowing carbon monoxide. A second powder was obtained from the National Bureau of Standards. The WC NBS Standard Reference Materials No. 276 was synthesized by direct reaction of the elements. Treibacher Chemische Werke of Austria supplied a solid solution of WC in the TiC cubic lattice, WC/TiC 70/30 (atomic ratio). The impurities in these powders are listed in Table 2.

Ultrapure water with a resistivity of 18 megaohm-cm from the Milli-Q water purifier of Millipore Corporation was used with

Table 1. Mass Spectrographic Analysis of As-Received Starting Powders for TiC_xO_y System

	Powder					
Element*	$TiC_{.956}$	$TiC_{.940}$	$TiC_{.801}$	$TiC_{.720}$	$TiC_{.639}$	TiO
B	300	2000†	200	< 10	< 10	≤ 400
Al	---	20	90	100	100	200
Si	20	40	200	70	400	700
P	---	----	<10	---	---	100
S	---	< 60	100	< 70	<100	≤ 80
Cl	---	90	300	100	80	100
K	---	90	70	10	30	300
Ca	20	50	300	30	< 50	200
V	20	----	---	----	----	-----
Fe	70	20	400	50	70	600
Ni	---	----	---	----	----	60
Cu	---	----	<10	300	----	< 20
Zn	---	----	---	80	----	-----
Zr	50	----	30	----	----	90
Nb	10	----	9	10	----	20
Ta	---	80	<10	10	< 20	< 10
W	---	30	---	----	----	-----

*Impurity levels given in ppma. Accuracy is ÷/× a factor of 5.
†From boron carbide mortar and pestle.

Table 2. Chemical Analysis of As-Received Tungsten-Containing Carbides

Element	Powder		
	WC/TiC 70/30*	WC NBS*	WC 165†
Mg	Interference	600	50- 500
Al	20	100	--------
Si	< 90	300	50- 500
P	30	100	--------
S	100	300	--------
Cl	40	20	--------
K	---	400	--------
Ca	80	200	500-5000
V	10	10	--------
Cr	90	30	100-1000
Fe	500	100	500-5000
Co	200	---	--------
Cu	----	8	50- 500
Mo	500	500	50- 500
Ag	----	---	50- 500
Ta	500	---	--------

*Mass spectrographic spark source analysis in ppma. Accuracy is ÷/× a factor of 5.

†Atomic emission spark source analysis in ppmw. Kindly supplied by P. N. Ross, Jr.

Ultrex grade sulphuric acid to prepare the electrolyte. The Ultrex grade sulphuric acid contained 10 ppm non-metallic and 50 ppb metallic impurities.

B. Powder Preparation

Powders in the titanium carbide and titanium oxycarbide systems were prepared by a method similar to that used by Naumenko [35] for the carbides and by Alyamovskii and coworkers [36,37] for the oxycarbides. To prepare titanium carbide and titanium oxycarbide compositions, an already existing titanium carbide was altered by additions of pure, small particle size carbon and titanium monoxide. This allowed titanium carbide and oxycarbide powders to be formed with relatively little diffusion or chemical reaction taking place. Homogeneous powders close to the desired composition could be formed with low reaction times, following which only 1-3 hr of labor were necessary to reduce the hardened billet to a powder.

The powders to be reacted were mixed in a plastic vial containing fresh plastic balls by a Spex mixer for 10 min. The powder was then loaded and compacted by hand in an outgassed high-purity graphite crucible with lid. The mixtures were fired in a Brew vacuum furnace using a Sylvania tungsten mesh element and tungsten heat shields. Vacuum of at least 5×10^{-6} torr was obtained before proceeding to outgas the mixture at 900°C for 1 hr. At this point, since titanium carbide loses titanium selectively by volatilization, for low carbon compositions ultra-high purity argon was admitted to suppress composition change. The mixtures were reacted at 1550°C for 2-3 hr. for the carbide and 10-20 hr. for the oxycarbide after which furnace power was turned off and the sample allowed to cool in vacuum to room temperature. Samples were broken and ground by hand in a boron carbide mortar and pestle since contamination from the normal tungsten carbide shaker could not be tolerated. Powders were passed through clean nylon 400 mesh screens and stored in a dessicator.

C. Pressure Differential Scanning Calorimetry

The use of differential thermal analysis is not a new technique for examining catalysts. As the term "calorimetry" implies, the calorimetric cell is designed to detect quantitative heats of reaction, rather than only qualitative differential temperatures, through better insulation and more careful construction than the normal DTA cell. The integrated area under the measured differential temperature curve is directly proportional to the total differential heat input. This technique is appropriate to this study because of the small quantities of catalyst powders available and their suspected relatively low activity.

Chemisorption of hydrogen from the gas phase on carbide powders is investigated. The instrument used is a DuPont Model 900 Thermal Analyzer with a DuPont Pressure DSC Cell attached. The technique [38] involves switching from an inert atmosphere over the catalyst to a high pressure of hydrogen at the desired temperature. This allows a rather high sensitivity to the heat of chemisorption on the catalyst since the adsorption takes place rapidly giving a large differential heat change.

High pressure regulators were attached to cylinders of special purity Linde "Zero" grade helium and hydrogen. Copper tubing of 1/8 in. diameter was run from each cylinder to the inputs of a Hoke three-way ball valve to allow instantaneous gas switching. The output from this valve was fed into the PDSC cell which had its own fine-thread (14 turn) high-pressure outlet needle valve with which fine adjustments to the flow from the cell could be made. A calibrated flow meter allowed monitoring of outlet flow. The common part of a three-way ball valve was connected to another cell-access valve, a coarse-threaded stop valve which is normally closed. A cylinder of Linde "High Purity" grade oxygen was attached to one branch of the three-way valve to allow admission of oxygen to the catalyst, while the other branch allowed rapid exhaust of the cell.

Samples weighing from 6-70 mg were loaded into gold pans which were made from 10 mil foil and were about 6 mm diameter and 1.5 mm deep. Thermal mass of the loaded sample pan was matched in the reference pan by a specific amount of gold wire. After being sealed in the cell, the cell atmosphere was purged with a high flow of helium for 15 min. Pressure of the helium was adjusted to 150 psia, and the flow was decreased to 20 ml/min. The cell was then heated rapidly to within 15°C of the desired temperature, and a heating rate of 5°C/min. was then established. A strip chart recorder (Honeywell, Electronik 194) was activated to monitor the temperature rise, ΔT, and chart speed and sensitivity were adjusted to properly expand the expected signal. Coincidentally the X-Y recorder of the DuPont Model 900 was started with appropriate scale settings. At the desired temperature the three-way valve was switched to allow hydrogen at 200 psia to be adsorbed on the sample. When the tracings returned to baseline the run was stopped and the cell was allowed to cool to 25°C in helium. Oxygen at 10 psia was admitted to observe whether this would clean the hydrogen from the catalyst surface by forming water. Many runs could then be made on one sample with alternate adsorption of oxygen. Calibration of measured curve areas was accomplished by measuring the melting endotherm of indium under hydrogen at 200 psia with the identical flow rate and heating rate.

D. Electrochemical Measurements

Potentiostatic and potentiodynamic experiments were performed in which a potential across the catalyst-containing electrode is applied, and the current produced by the catalyzed oxidation of hydrogen in acid solution is measured. The current density at an appropriate voltage represents the activity for comparing different catalysts.

The measurement cell contains the standard three-electrode configuration as shown in Fig. 2. In one chamber the porous,

Figure 2. Teflon electrochemical cell.

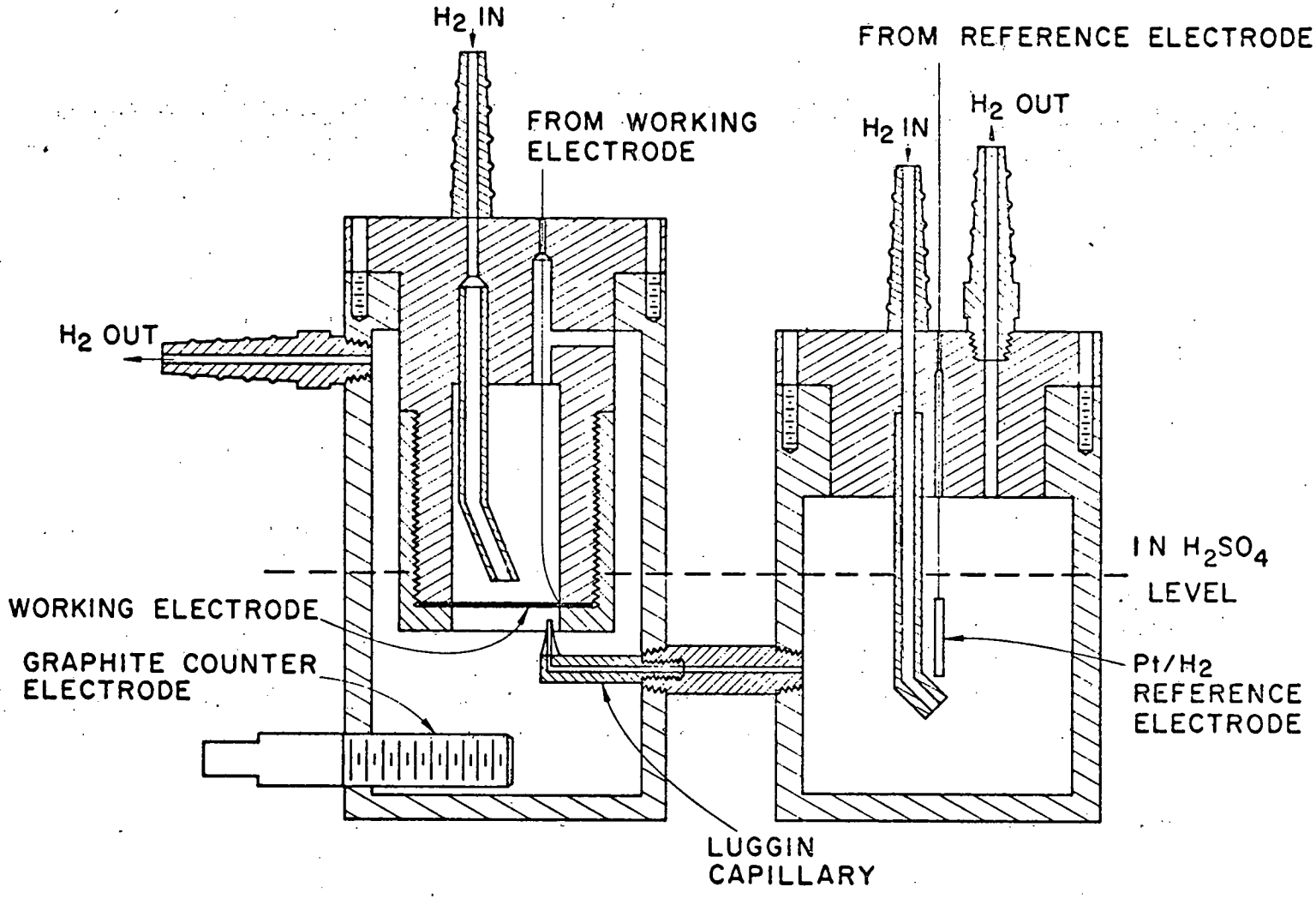
H_2 IN
FROM REFERENCE ELECTRODE
FROM WORKING ELECTRODE
H_2 IN
H_2 OUT
H_2 OUT
IN H_2SO_4 LEVEL
WORKING ELECTRODE
GRAPHITE COUNTER ELECTRODE
Pt/H_2 REFERENCE ELECTRODE
LUGGIN CAPILLARY

hydrophobic working electrode containing the catalyst powder is placed in contact with a gold foil disc current collector and sealed to the holder, with a threaded teflon cap, with one side exposed to hydrogen gas at 1 atm. and the other side in 1 N H_2SO_4 electrolyte. In the same chamber is the graphite counter electrode. The platinum-black electrode in the second chamber reaches a reference voltage defined as zero volts in 1 N H_2SO_4 with 1 atm. hydrogen bubbling over it. This potential is brought to the catalyst surface by the Luggin capillary. A buffer amplifier in the instrumentation stops current from flowing through this electrode so that the capillary acts as a voltage probe. A potential is selected at the potentiostat (Princeton Applied Research, Model 371 Potentiostat) to be applied across the catalyst surface.

The actual potential between the catalyst surface and the Pt/H_2 reference electrode is sensed by a feedback loop in the potentiostat, which corrects this voltage if it does not equal the desired voltage by supplying additional current between the graphite counter electrode and the working electrode. This system allows the entire voltage to be dropped across the surface of the catalyst and simultaneously measures the current crossing the electrode surface. Output from the potentiostat representing applied voltage and reaction current was fed to the X- and Y-axis, respectively, of a Houston Instruments Model 2000 Recorder. Digital voltmeters (Keithley, Model 163) in parallel with the signals allowed easy monitoring of the process. Slow voltage sweeps and programming were provided by either a voltage ramp generator (Elscint, Model ABA-26) or a voltage programmer (Princeton Applied Research, Universal Programmer, Model 175). Hydrogen for the cell (Linde "High Purity" grade) was deoxygenated by passing through an oxygen and water eliminator (Airco, Model 98LP Oxygen and Water Eliminator), reducing oxygen to less than 0.1 ppm.

A calibrated flow meter allowed adjustment of the hydrogen flow rate. A gas bubbler with a fritted glass disc moisturized the hydrogen to avoid concentration of the electrolyte in the cell. Hydrogen was admitted to the two compartments of the cell as shown in Fig. 2 and outlet bubblers eliminated the diffusion of oxygen back up the outlet lines.

To begin a run, the two compartments of the cell were half filled with 1 N H_2SO_4. Linde "Prepurified" grade argon was purged through the two compartments for 1 hr. to rid the electrolyte of trapped oxygen. Meanwhile the catalyst electrode was laid on the end of the working electrode holder in contact with the gold foil current collector, with the catalyst side of the electrode facing out. The teflon end cap was threaded on, sealing the rear of the electrode from the electrolyte. The working electrode holder and the Pt/H_2 electrode holder were connected to their inlet gas bubblers and hydrogen was allowed to purge the holders for several minutes to remove oxygen. The argon purging was stopped and the outlet of the reference electrode compartment was briefly plugged while the holder was forced down into the compartment. This pushed the electrolyte through the Luggin capillary sweeping out trapped air which would cause an open circuit in the catalyst-reference electrode line. Both holders were sealed in their compartments with stainless steel screws. The rest potential (zero current) is monitored with the potentiostat and the electrode was allowed to wet with electrolyte at H_2 open circuit for from 2-12 hrs. A preliminary anodic sweep of voltage at 1mV/sec to 300 mV (SHE) identified the general behavior of the catalyst in hydrogen. If the electrode was found to be active, several more sweeps were performed to determine reproducibility. The electrode was then scanned to various voltages, where the potential was held for 2 min. to allow the recording of steady-state curves. These values were normalized to the real surface area of sample exposed and compared between different samples to determine relative catalytic activity.

The catalyst electrodes were roughly 40 mm diameter, although the actual diameter of the region covered by catalyst is 30.5 mm. The substrate was required to be electrically conductive, but porous, to allow H_2 penetration from the back side of the electrode. It also had to be hydrophobic, to limit the length of diffusion channels and to prevent wetting through by the electrolyte. The final requirement was to be pinhole free, so that all known loading could be directly filtered onto the substrate without loss.

Fibrous carbon paper of 15 mil thickness was supplied by United Technologies Corporation. This paper was not pinhole free or hydrophobic. To remedy this, carbon black (Vulcan XC-72, Cabot Corp.) and teflon dispersion (TPE 30, DuPont Chemicals) were flocked together and filtered onto the electrode in two layers. For the first layer the paper was wet with isopropanol and a flock of 23 mg carbon and 7.5 µl TFE 30 with 5 ml water was filtered onto its surface. While wet, this layer was placed on filter paper and pressed with a roller. This was dried at 190°C and sintered 1 min. at 335°C in a vacuum tube furnace. This surface was badly cracked. This was dipped into 20 w/o PTFE dispersion, blotted, dried, and sintered for 1 min. This sealed many of the small cracks. This paper was placed in the filtering device, wet with isopropanol, and a second block of 17 mg carbon and 6.1 µl TFE 30 was filtered onto the disc. This was dried at 120°C, after which, while hot, the paper was rolled with a clean roller. The sintering of the teflon was done at 335°C for 10 min. A number of these papers were adequate except for a small number of pinholes, which caused loss of sample on filtering. Late in this study a second type of carbon paper was used. Pinhole-free carbon paper made from pressed carbon black was obtained (Stonehart Associates, Madison, CT), in 5 in. × 5 in. FEP wetproofed sheets 15 mil thick. Although filtration loss with the paper was minimal, all signals measured were cut down by a factor of 10. The cause of this was thought to be an extremely heavy layer of FEP as wetproofing.

Catalyst electrodes were usually made with 10 mg/cm^2 (geom.), an optimized weight for structural integrity of the catalyst layer. This quantity of catalyst was placed in a beaker with 6 ml water and ultrasonically mixed with a small quantity of TFE 30. High surface area catalysts (WC 165) required 30 w/o TFE while low surface area powders were made with 5-10 w/o TFE. After filtration the catalyst electrodes were dried in air at 120°C. Since WC oxidizes in air at low temperatures, the vacuum tube furnace was adapted with flow connections to allow the electrode to be sintered in flowing argon (Linde "Ultra-High Purity" grade) at 335°C for 10 min.

E. X-Ray Photoelectron Spectroscopy

Surface chemical states of tungsten, carbon, and oxygen were investigated by X-ray photoemission for the WC 165 and WC NBS samples. These studies were performed by Surface Science Laboratories, Palo Alto, CA. A Hewlett-Packard 5950A ESCA spectrometer was used with monochromated Al Kα X-rays (1486.6 eV). Monochromating the X-ray source reduced the total X-ray exposure by two orders-of-magnitude, minimizing X-ray decomposition of the surface. The W 4f, C 1s, and O 1s core state regions were plotted as functions of binding energy of the photoelectrons. Binding energies were calibrated against the Au $4f_{7/2}$ line at 83.8 eV. The three regions of the spectrum were each fitted using a least-squares calculation procedure assuming the fewest number of lines that would give a good fit.

After initial spectra were recorded, samples were argon ion etched. The accelerating voltage of the beam was 3 kV, with an emission current of 15 mA. This gave a beam current of about 1/4 μA which was rastered over a 7 × 2 cm area, with < 600 μ spot size. These conditions produce an etch rate of 7 Å/min. on SiO_2. A WC 165 sample was etched 2, 15, and 40 min. respectively while WC NBS was only given a brief 1-2 min. etch. The same regions of the spectra were recorded after each etch.

Surface compositions were estimated from photoemission data. The conversion of signal intensities to relative atomic compositions was done by weighting the intensities by the inverse of the relative theoretical photoemission cross-sections. [39] For WC 165 an estimate was made of the contribution to the spectra of the surface contamination film.

F. Auger Electron Spectroscopy

Since AES uses an electron beam source and measures the current of emitted Auger electrons, this technique receives information only from the first 2-4 atomic layers. It is also known that this technique may in simple cases be able to give quantitative information about the composition of the surface layer of a material. Since TiC_x and TiC_xO_y might represent one such simple case, it was decided to test the ability of AES to give a quantitative description of carbide surfaces and to test the possible preferential sputtering of surface atoms by the argon ion etching beam. It was hoped to correlate this information to the catalytic behavior of the carbides. Surfaces of powders of WC NBS and WC 165 were examined initially and after brief etches.

The instrument used was a scanning Auger microprobe (Physical Electronics Industries, Inc., Model 545, with some modifications). The standard procedure was used to load the samples and tune the CMA to the 2 kV elastic electron peak. The measurements were made in an argon partial pressure of 5×10^{-5} torr to allow alternate sputtering and spectrum runs to be rapidly performed. Samples were examined initially and after various etching times up to 30 min. The parameters used in gathering the spectra are given in Table 3. The elastic peaks for several samples were also recorded at a primary electron energy of 1.5 kV to observe energy loss phenomena in order to better interpret results found for these samples.

Table 3. SAM Instrumental Parameters

E_p = 3 kV	I_p = 16.1 μA
V_{MOD} = 3 V	V_{MULT} = 700 - 850 V
RC = 0.1s	Sen = ×40
EV/in. = 50	Rate = 1 eV/s
V_{Ar^+} = 3 kV	I_{Ar^+} = 30 mA

Powder samples were prepared 1/2 to 1 hr ahead of time. Oxygen-free copper foil 10 mil thick was cut into 8 × 8 mm squares and rinsed in methanol. Enough powder to cover an area 3 × 3 mm was sprinkled on the foil and pressed in by hand with a clean glass slide. Copper was chosen because it had one minor peak within the energies observed but did not interfere with any peaks of the sample. This allowed monitoring of possible contributions to the carbon or oxygen lines from contamination on the substrate.

G. Electron Spin Resonance

Electron spin resonance is a technique often used to study active sites and catalytic reaction intermediates with unpaired electrons. Since one model for carbide catalysis proposes creation of an O^- ion, WC 165 and WC NBS samples were examined for ESR signals.

The instrument used was an X-Band EPR (Varian E-9 EPR spectrometer) with an E 101 microwave bridge operated at about 9.1 GHz in these runs. For this work the low temperature cooling jacket was always left in place. The sample was loaded in an ESR quartz tube to a height to fill the cavity and the tube was placed in the cavity. The klystron was first tuned and the reference arm was adjusted to give the proper biasing of the detector diode. The sample was run at room and liquid nitrogen temperatures. The entire range of magnetic field (0-10 kG) was examined for energy adsorption by the sample from the microwave field. The WC 165 sample was also etched in warm HCl in an attempt to remove impurities before one set of runs.

Peak g-values were calculated by the standard resonance formula:

$$h\nu = g\beta H_0 \quad , \tag{2a}$$

or

$$g = \frac{0.71449}{H_0(\text{kG})}\, \nu_0(\text{GHz}) \quad . \tag{2b}$$

H. Other Spectroscopy Techniques

An 180° magnetic deflection mass spectrometer (AEI MS 10, AEI, Ltd.) was used in an attempt to investigate the desorption behavior of hydrogen chemisorbed on the carbides at room temperature. This system has been described previously.[40] The sample chamber vacuum system was capable of reaching 1×10^{-5} torr in 2 hrs, pumping on an outgassed sample. When closed the spectrometer chamber was able to maintain 2×10^{-9} torr. WC NBS and several titanium carbides and oxycarbides were tested.

A high purity alumina boat was loaded with 5-10 g of sample. The boat was pushed to the end of a closed-end alumina tube which had been sealed to a Conflat (Varian Associates, Inc.) flange by means of a Viton O-ring quick-disconnect. This flange was attached to the vacuum system and evacuated with a liquid-nitrogen trapped mechanical pump and a liquid-nitrogen trapped diffusion pump. After 4 hrs the sample was heated to 800°C at 10°C/min. The outgassing was monitored as a function of temperature on an X-Y Recorder. The sample was cooled to room temperature and 20 psia of hydrogen (Linde "Ultra-High Purity" grade) was admitted for 1 hr. This was pumped out at 22°C for about 2 hrs., when the vacuum reached 1×10^{-5} torr. The temperature was then ramped at 10°C/min. to about 750°C, and both pressure in the sample chamber and the mass spectrometer hydrogen signal recorded as a function of temperature. Values of m/e of 18, 29, and 44 were recorded individually at various temperatures by manually retuning the accelerator voltage during the run.

No spectra could be attributed to hydrogen desorption from WC NBS or any titanium-oxycarbide by this technique. Due to this negative result this finding is reported in this section.

An IR spectrometer (Beckman, Model IR 12) was used to examine WC 165 to determine whether this technique might be used to watch the formation of W-H, C-H, or O-H bonds during chemisorption. As an initial experiment WC-KBr pellets were tested in transmission. In the wavenumber range 500-4000 cm^{-1} WC 165 was opaque

to the IR beam. This is reported here for completeness.

I. Bulk Chemical and Structural Characterization

Combustion analysis for total carbon and oxygen in the carbide powders was performed by LECO Corp. All reported analyses are the average of 2-4 values. In addition, since the titanium carbides and oxycarbides dissolve in concentrated HNO_3, these samples were tested for total titanium content by spectrophotometric analysis by J. Baker of the analytical chemistry facility in the MRL. Analyses of samples of titanium oxycarbides for which the sums of the components did not agree were considered suspect, and these samples were not used.

Powders which had been prepared by reacting at high temperatures were scanned for completeness of the reaction by using an X-ray diffractometer. Unreacted phases and poorly-formed $K\alpha_1$-$K\alpha_2$ peaks at high 2θ showed the sample must be pulverized and re-fired. An X-ray powder camera, diameter 114.59 mm, was used to determine the lattice parameter of the homogeneous powder. The X-ray source was a copper tube operated at 30 kV and 15 mA, with a nickel filter. Nelson-Riley analysis was used with a least-squares fit to obtain values for lattice parameters.

J. Surface Area Measurements

The specific surface areas of all powders were determined using a static gas adsorption test based on the Brunauer, Emmet, and Teller (BET) physical adsorption theories.

The particular instrument used was a high-speed, single pressure unit (Micromeritics, High-Speed Surface Area Analyzer, Model 2205) using Linde "High Purity" argon as adsorbate. The manufacturer-stated accuracy was ± 3% and reproducibility was ± 0.5%.

The samples were weighed in the glass flasks and attached to the machine. The suggested procedure was followed and the sample was baked out at 225°C in flowing argon for 40 min.

The selected volume of the flasks automatically applied an approximate correction to the total area indicated for the adsorption at liquid-nitrogen temperature for only one pressure. The measurements yielded the highest accuracy when the total sample area was between 5 and 35 m^2.

K. Scanning Electron Microscopy

The scanning electron microscope (Japanese Electron Optic Co., Model JSM35C) was used to investigate powder morphology. WC NBS, WC 165, and several titanium carbides were examined. A metal stub was coated with aquadag and allowed to dry 5 min. The carbide powder was then sprinkled over the aquadag. Secondary electron imaging was used, with accelerating voltages of 35 kV for WC 165 and 25 kV for the other powders.

CHAPTER 3

RESULTS AND DISCUSSION

A. Bulk Properties and Surface Areas

The results of combustion and spectrophotometric analyses for carbide powders in this study are shown in Table 4. Titanium oxycarbides were found to lose substantial percentages of the total oxygen on firing. Carbon was also generally lost, but to a lesser degree. Data used to calculate the lattice parameter from a least-squares fit to the Nelson-Riley extrapolation in each case had a correlation coefficient, R^2, greater than 0.97, so that these lattice parameters may be considered to be very reliable. These values also agree quite well with oxycarbides of similar compositions in the literature,[36,37,41] so that the formulas listed in Table 4 are believed to be very accurate for the bulk.

It should be noted here that WC NBS has very low oxygen content in the bulk and is very close to stoichiometry. WC 165 on the other hand is low in carbon and high in oxygen in the bulk. A simple calculation indicates that if it is assumed that all the oxygen is in WC 165 as WO_3, then the composition of the remaining carbide is $WC_{1.02}$. This would imply that about 16% of WC 165 material is actually WO_3 and the rest is stoichiometric carbide. A second phase was actually observed by X-ray diffraction. Using the X-ray diffractometer, the two most intense lines of WO_3 were observed at very high gain. It is not felt that these peaks could account for 16% of the sample. There seem to be two ways to be about to account for the oxygen. One possibility is if the WO_3 was in the form of very small pickets in the carbide, perhaps due to inhibited or only partial carburization of the beginning oxide. In Fig. 2 SEM micrographs show the size and shapes of various carbides from this study. It can be seen (Fig. 2a) that there are many WC 165 particles below 0.1 μ.

Table 4. Characterization of Bulk Properties and Surface Areas of Carbide Powders

Sample no.	Carbon* content (w/o)	Oxygen* content (w/o)	Titanium† content (w/o)	Formula	Surface area (m^2/g)	Lattice parameter (Å)
WC 165	5.11	3.75	-----	$WC_{.857}O_{.473}$	10.5	------
WC NBS	6.31	0.172	-----	$WC_{1.03}O_{.0211}$	0.88	------
WC/TiC	10.36	0.0948	-----	$W_{.415}Ti_{.585}C_{1.00}O_{.007}$	0.51	------
$TiC_{1.00}$	20.10	0.0189	80.3	$TiC_{1.00}O_{.0007}$	0.57	------
$TiC_{.94}$	19.14	0.0317	-----	$TiC_{.944}O_{.0019}$	1.03	------
$TiC_{.86}$	17.68	0.596	82.5	$TiC_{.863}O_{.0022}$	1.06	------
$TiC_{.80}$	16.60	0.743	83.8	$TiC_{.801}O_{.0269}$	1.53	------
$TiC_{.72}$	15.25	0.155	-----	$TiC_{.720}O_{.0055}$	0.71	------
$TiC_{.64}$	13.81	0.064	-----	$TiC_{.639}O_{.0022}$	1.04	------
2B	15.83	3.33	80.1	$TiC_{.781}O_{.123}$	0.46	4.3196
6	7.97	12.14	78.5	$TiC_{.400}O_{.455}$	0.57	4.2891
7	17.13	2.10	80.8	$TiC_{.846}O_{.078}$	0.46	4.3238
8	15.63	3.08	80.8	$TiC_{.772}O_{.120}$	0.63	4.3192
9	15.34	4.18	80.0	$TiC_{.765}O_{.164}$	0.47	4.3168
10	18.15	1.42	80.7	$TiC_{.893}O_{.049}$	0.50	4.3229
11	13.02	3.00	84.4	$TiC_{.618}O_{.107}$	0.60	4.3090

*LECO Combustion analysis.
†Spectrophotometric analysis. Estimated accuracy ± 1.6 w/o.

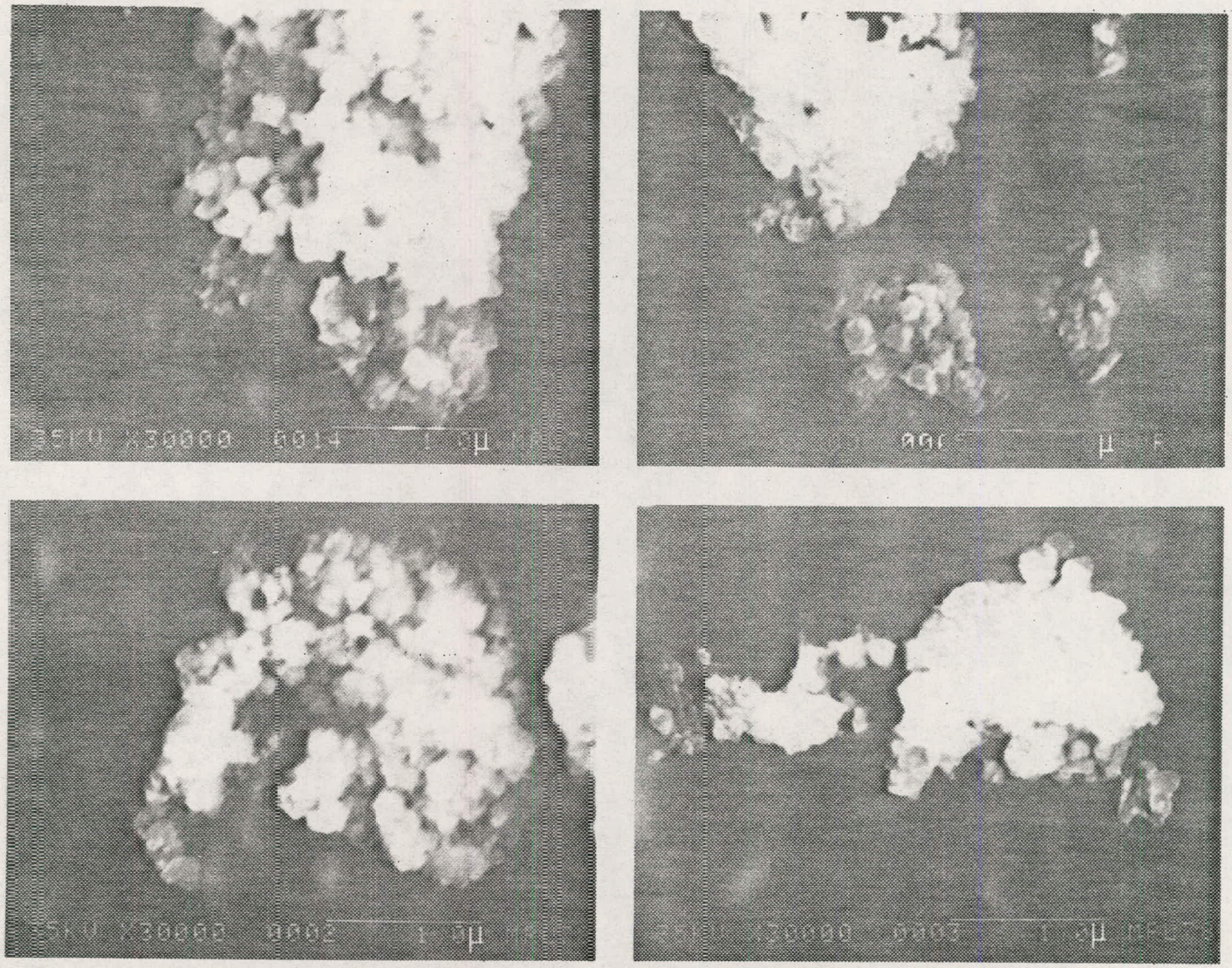

Figure 3a. SEM micrographs of carbide powders. (A) WC 165.

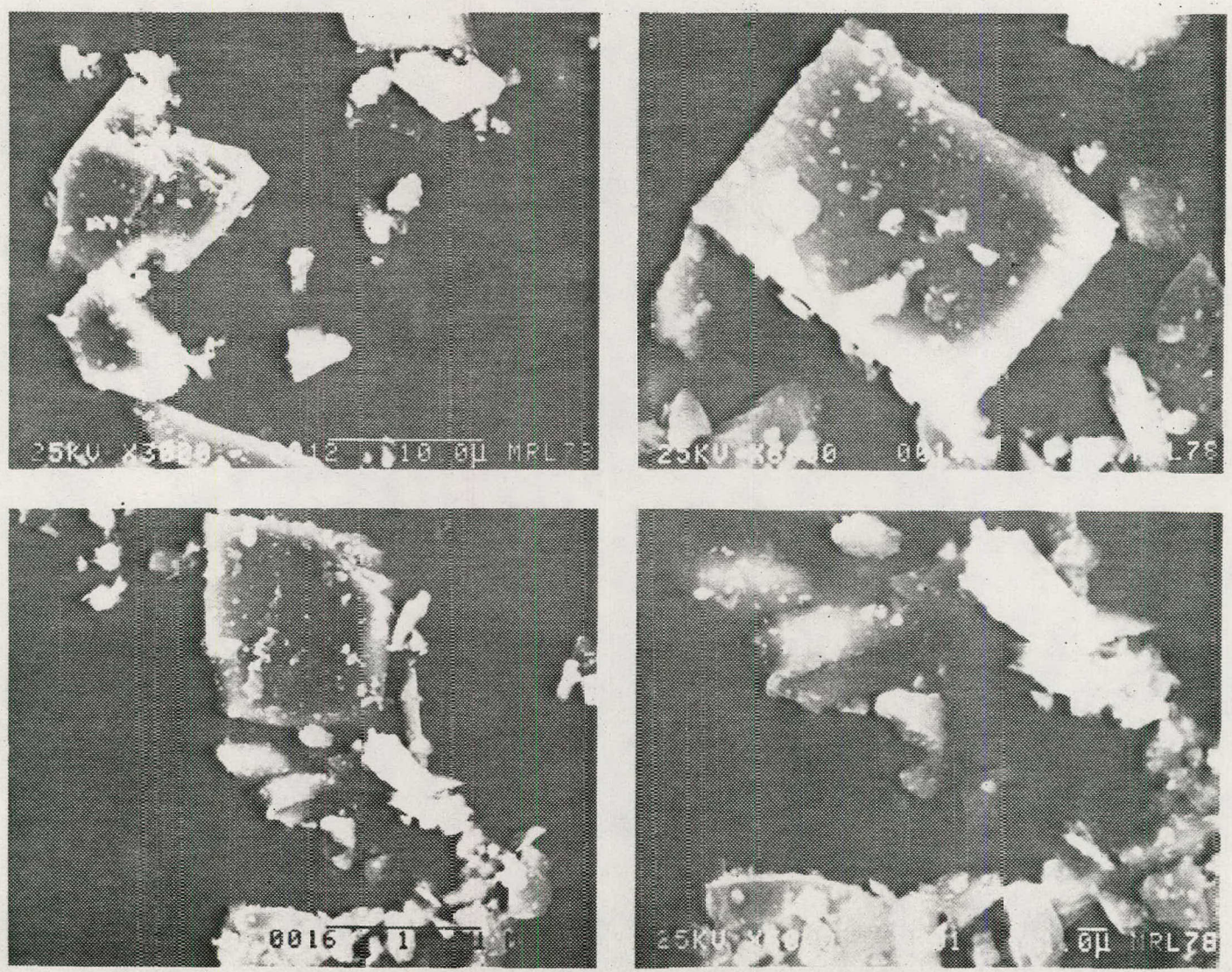

Figure 3b. $TiC_{.944}O_{.0019}$.

Figure 3c. WC NBS.

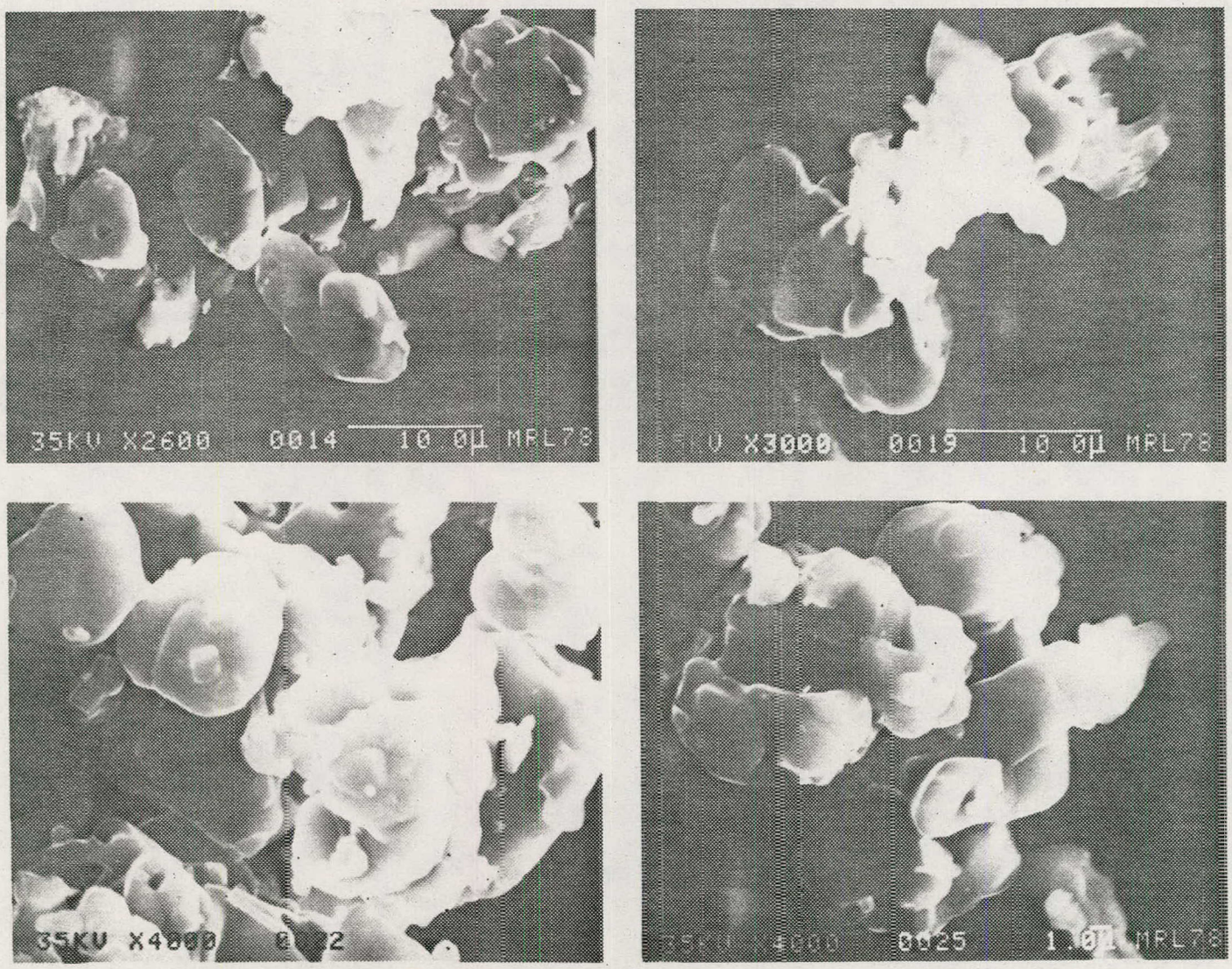

Figure 3d. Sample No. 9, $TiC_{.765}O_{.164}$.

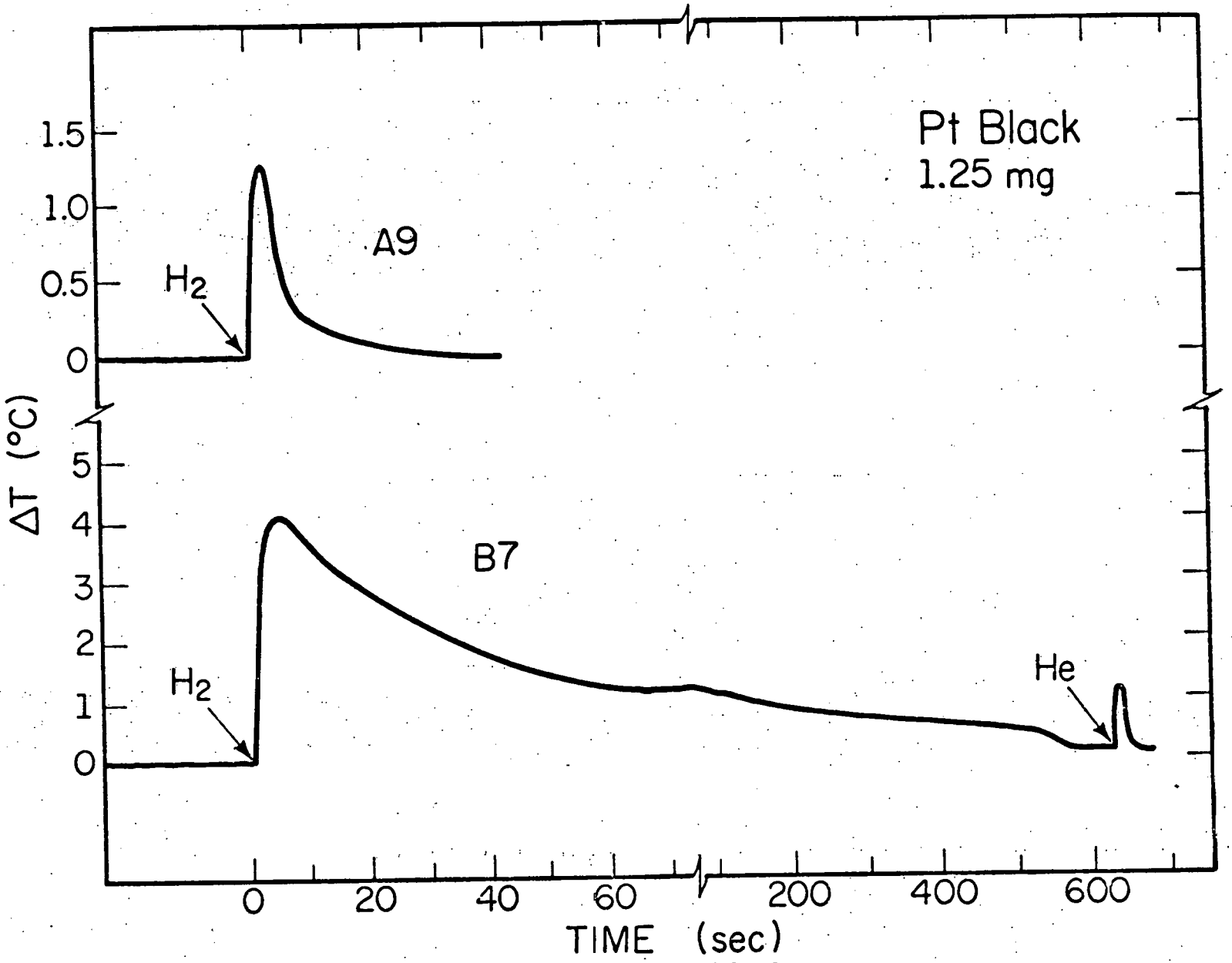

Figure 4. PDSC test of Pt black.

Using the surface area from Table 4 and the formula $\bar{d} = 6/S\rho$ where $\rho = 15.63$ g/cm^2, one obtains an average particle size of 0.04 μ or 400 Å. If the WO_3 pockets are even one-fourth this size, the X-ray diffraction lines would become so broad that they would be indistinguishable from the background.[42] This may be what is found here. On the other hand, while some of the oxygen is combined as WO_3, some of it is likely to be substituted into the lattice [42] as is the case for the oxycarbides of this study. If these combustion analyses are correct, however, this cannot account for most of the oxygen.

Figure 2b shows morphologies of other carbide powders. $TiC_{.94}$ is a ground single crystal, and well-defined crystal plane faces are seen. For WC NBS (Fig. 2c) the particles are very closely sized and seem to have an average particle diameter of just under 1 μ. The surface area from Table 4 gives an average particle diameter of 0.44 μ. Many particles of WC NBS are seen to have sharp hexagonal or triangular shapes. Particles of Sample No. 9 (Fig. 2d) average the largest in size of the samples observed. Samples were opaque to the transmission microscope without further thinning.

B. Chemisorption Behavior

Figure 3 shows the progress of two separate runs determining the total differential change in temperature between 1.2 mg of platinum and a thermally matched weight of alumina when helium at 150 psia is switched to 200 psia of hydrogen at 75°C with an initial helium flow rate of 20 ml/min. For these cases the temperature was scanned at about 14°C/min. Run B7 was made under conditions which were later seen to produce curves on the carbides such as that seen for WC 165 in Fig. 4. It is believed the behavior shown in Fig. 4 is not due to chemisorption. Peaks such as these for the carbides were not observed if the PDSC cell was very extensively purged with helium (25 min. purging

through both gas outlets) before each run was begun. Similarly for platinum, the smaller heat was recorded if the long initial purging at high flow was maintained or if the system was gently pumped. The titration of adsorbed oxygen on platinum by hydrogen is well-known [44] and reduction of additional PtO oxide layers might evolve heat in this experiment. The long "shoulder" in run B7 is particularly suspect.

Heats normalized to total sample area are calculated from the equation:

$$\Delta H = \frac{EA\Delta T_s r}{mS} \quad , \tag{3}$$

where E is the calibration coefficient determined for In with the same equation and the known heat of melting for In, A is the area under the ΔT — time curve, ΔT_s is Y-axis scale factor, r is the chart speed, m is the sample weight, and S is specific surface area. If 1.12×10^{19} sites/m^2 is assumed for platinum black [45] and H/Pt = 1, then for a surface area of 42.2 m^2/g, the heat of chemisorption (E_a in Fig. 1) from Run A9, is found to be 84 kcal/mole, yielding a site-averaged Pt-H bond strength from Eq. (1) of 94 kcal/mole. This value of E_b is high compared to the usually accepted value of 65 kcal/mole.[5] However, it is not inconceivable that the stoichiometry of the chemisorption reaction on platinum at 200 psia might shift to H/Pt = 2, which would account for this high value of E_b. It can be expected that PDSC will allow an approximate estimate of heats of chemisorption, dependent on assumptions of site densities and reaction stoichiometry, particularly when proper pretreatment of the catalyst powder is used. Relative values of total heat of adsorption on similar carbide materials should be especially reliable.

Figure 6 shows representative runs on WC 165 for 75°C, 100°C, and 200°C after purging 25 min. with helium at 24°C. The initial endothermic blip is due to the pressure surge into the system and a mild asymmetry in the cell design.

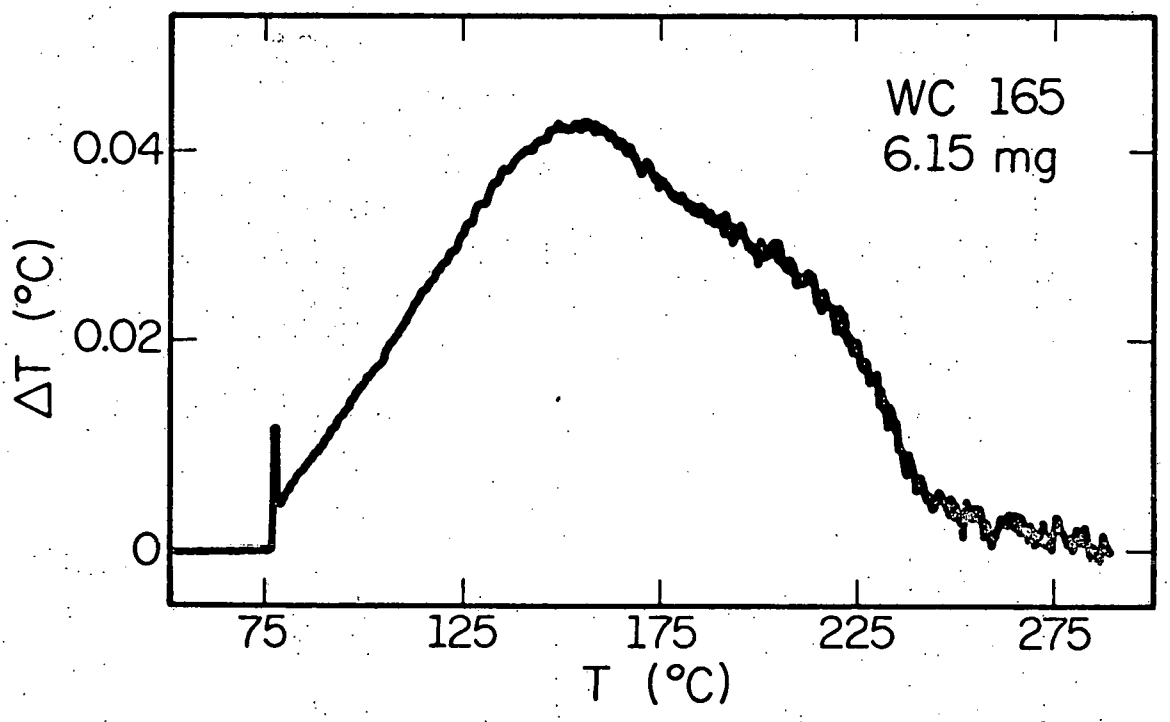

Figure 5. PDSC test with inadequate purging.

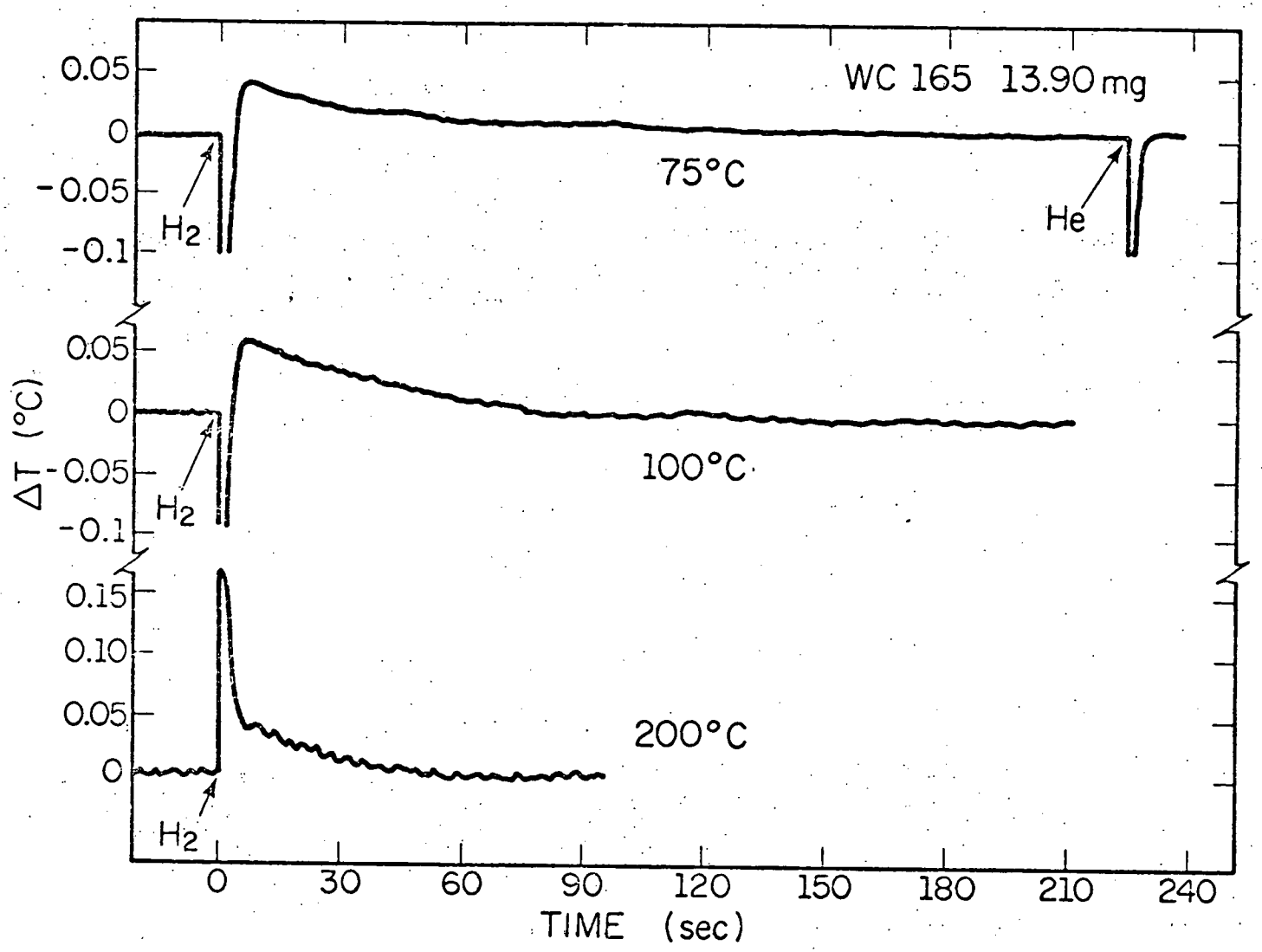

Figure 6. Temperature behavior of chemisorption on WC 165.

On the 75°C run helium was admitted at 250 psia after the trace had returned to baseline in order to check that the observed exotherm was not an additional pressure artifact. An immediate second run on the sample showed no heat evolution, indicating the adsorption sites were full. Adsorption of oxygen on WC surfaces which had previously adsorbed hydrogen followed by evacuation, has previously been seen to clean the WC surface for a new hydrogen chemisorption.[1,46] This was observed in the present study and was used to allow running of the same sample to different temperatures and to conserve our small supply of WC 165. A series of runs on samples of different weight showed that the heat scaled with amount of sample. Figure 7 shows an example of one such test.

Levy and Boudart [1] estimated from volumetric adsorption measurements that 22% of the surface of their WC powder was involved in water formation for their experiments at 25°C. The proper site density depends on the nature of exposed crystallographic planes. However, if a typical value of 1.2×10^{19} atoms/m^2 is assumed, then we will take a value of 2.4×10^{18} sites/m^2. Using an average of the ΔH values found at 75°C (0.1 cal/m^2) and assuming the chemisorption is dissociative, values of E_a = 46 kcal/mole and E_b = 75 kcal/mole are found for those sites. The W-H binding energy for the metal is 75 kcal/mole.[5] For the roughness of this estimate it must be assumed that this exact quality is in some part coincidence. However, this is still highly interesting. If the findings of Levy and Boudart are ignored, and the assumption made that all the tungsten atoms or all the carbon atoms can be sites at these high pressures, an average energy of adsorption for hydrogen becomes E_a = 20 kcal/mole.

The change in adsorption behavior with temperature of adsorption for WC 165 can be seen in Fig. 6. At $T \geq 75°C$ the curves become initially larger and return to baseline more quickly. The total heat of chemisorption, ΔH, is the summation of heats of adsorption per site ($\frac{1}{2}E_a$) at each site. A plot of ΔH with

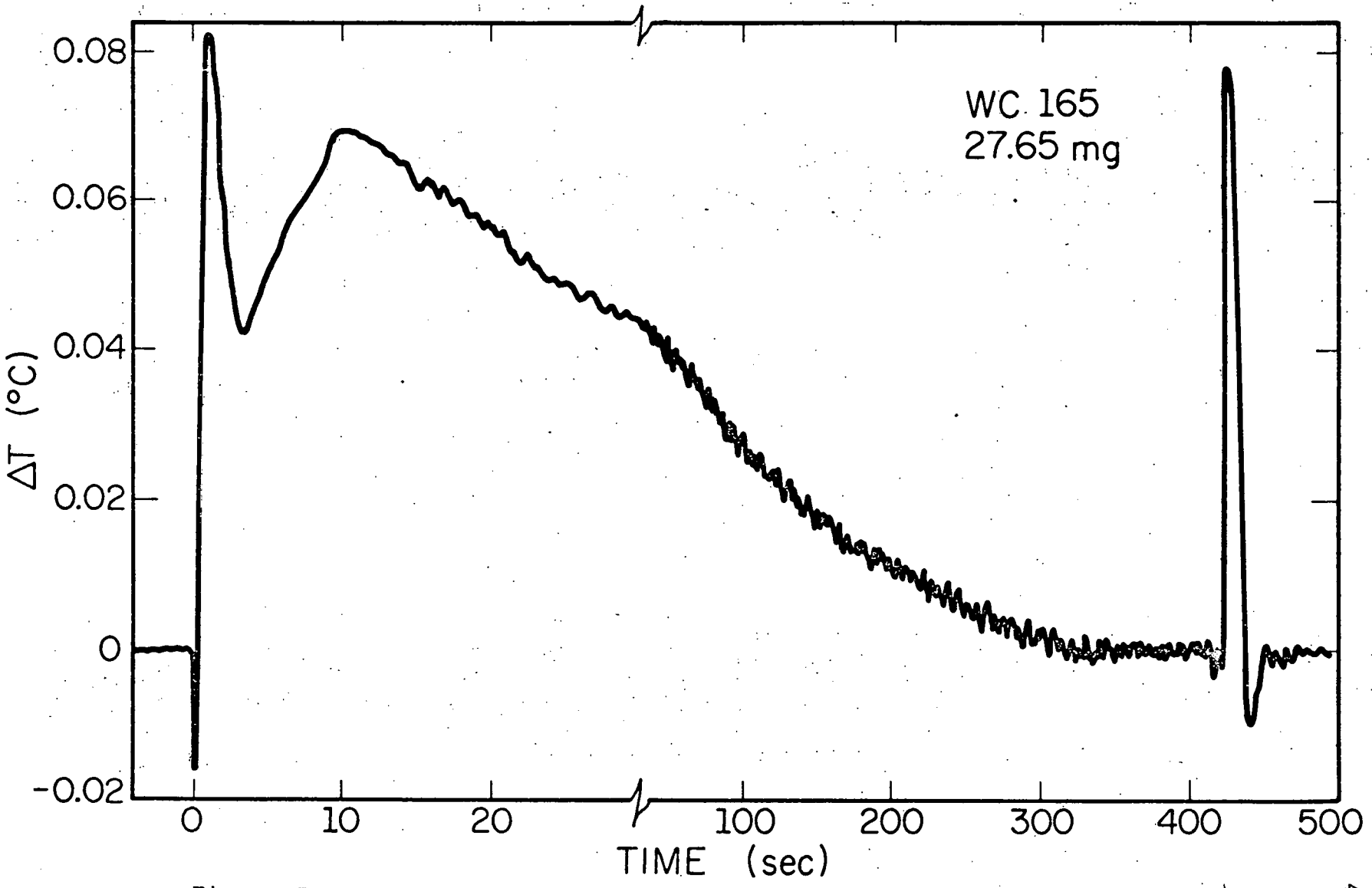

Figure 7. PDSC test for 27.65 mg WC 165. Initiated at 75°C.

increasing temperature for WC 165. If the assumption is made that E_a is constant with temperature, then Fig. 8 is tracing the changing coverage, θ, of the surface. Although the value of the slope gives E = 3.16 kcal/mole, unfortunately this cannot be easily interpreted since the technique presented here is an adsorption method although desorption is clearly taking place.[2] Adsorption and desorption processes are clearly competitive from 75°C to 275°C, where no adsorption is found.

Adsorption on WC NBS was not observed. An estimated upper limit from this work on the adsorption heat gives 0.02 cal/m^2 compared to the value of 0.1 cal/m^2 for WC 165, a factor of 5. This factor of 5 may occur by either a decreased number of active sites or the lower value of E_a. Ross and Stonehart [46] found in volumetric adsorption studies that certain WC powders adsorbed considerably less hydrogen than others, so that for WC NBS fewer sites adsorbing hydrogen seem likely.

Curves such as that found in Fig. 9 were typical of the adsorption in the titanium oxycarbide system. No recognizable adsorption curves were found. Curves such as that for $TiC_{.400}O_{.455}$ in Fig. 9 are not understood. The possibility exists that an exothermic reaction is taking place which is dependent on pressure. However, substitutional oxygen and carbon vacancies do not effect the adsorption of hydrogen on titanium carbide within the sensitivity of this experiment.

C. Hydrogen Oxidation Catalysis

The results of this part of the study establish the relative activity of the carbides for hydrogen oxidation. These results fall into two classes: those for the pure tungsten carbides and those for the cubic titanium carbide system.

Figure 10 shows a typical curve produced by a potentiodynamic scan on a tungsten carbide electrode. In this case the slight

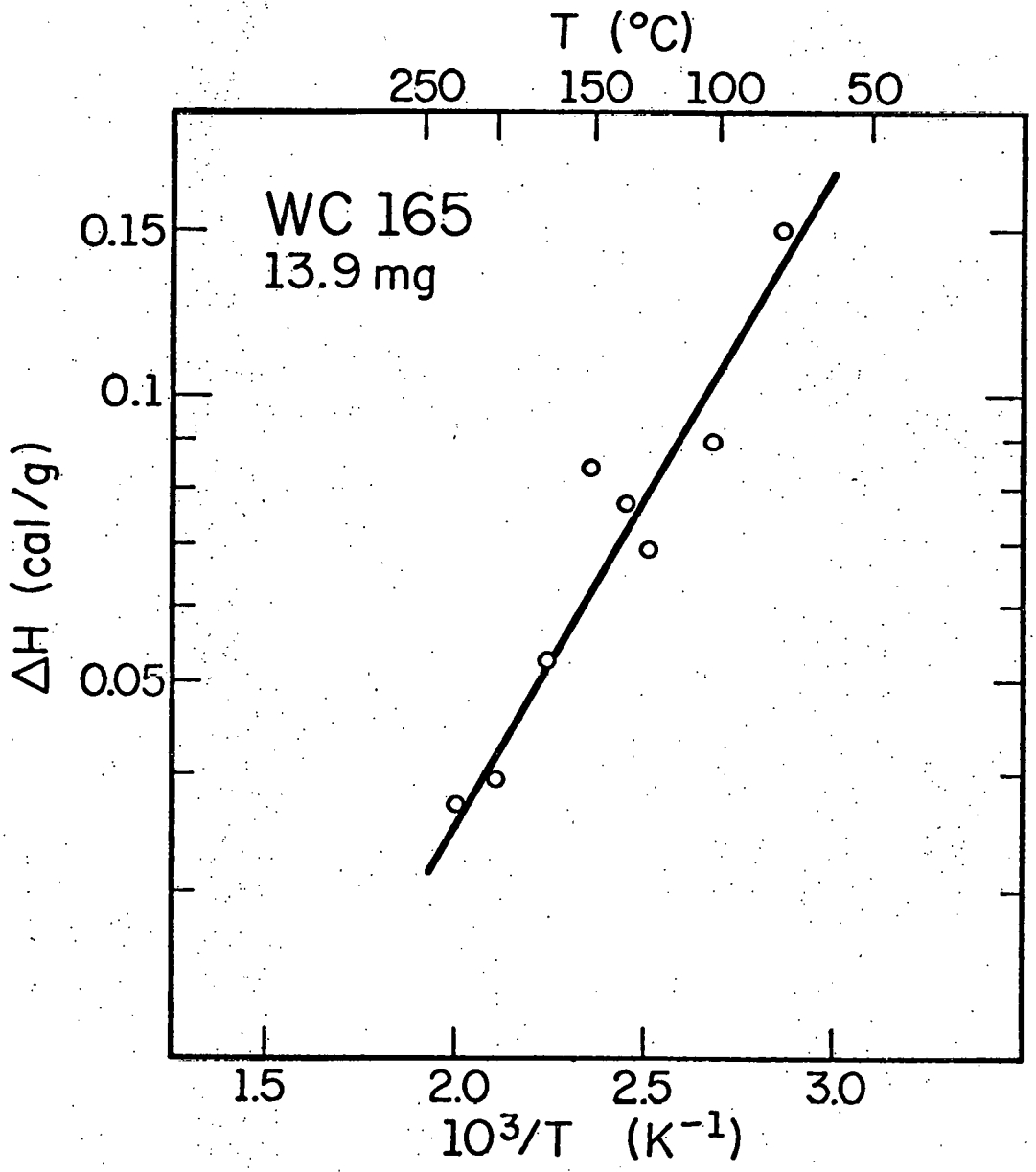

Figure 8. Total chemisorption heat as a function of temperature for WC 165.

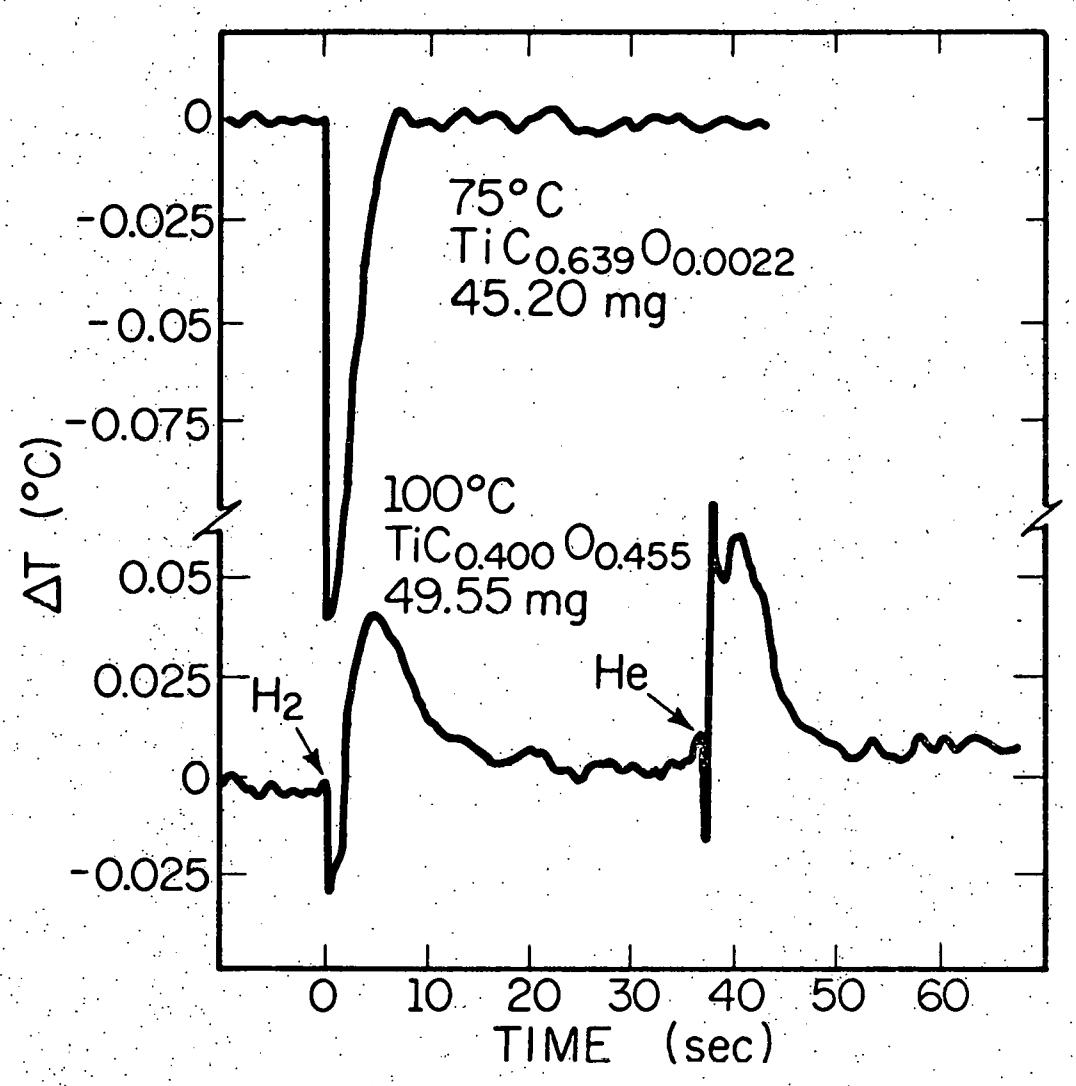

Figure 9. Typical PDSC tests for TiC_xO_y.

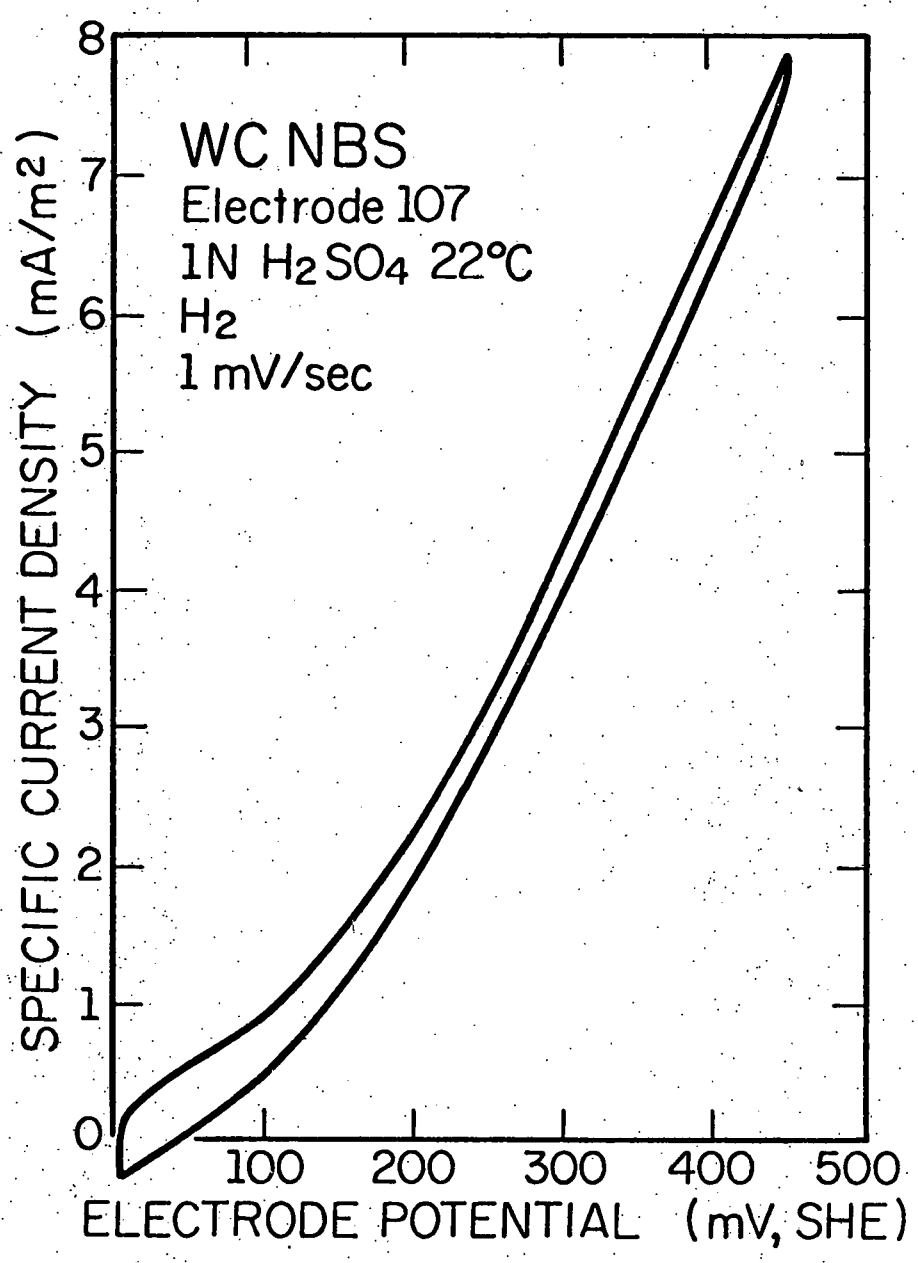

Figure 10. Potentiodynamic scan on WC NBS, electrode 107.

opening or hysteresis of the curve is due only to the rate of scan being somewhat too fast for the reaction to reach steady-state. This type of curve is representative of a continuous Faradaic reaction. The rest potential, E_o, was typically 9 mV for all tungsten carbide electrodes. E_o is characteristic of the equilibrium balance of all the reactions proceeding simultaneously on the surface. In this case it indicates hydrogen oxidation to be the dominant reaction near zero electrode potential.

The current at one voltage increased through several successive scans, slightly more for WC NBS than for WC 165. Both tungsten carbides were stable to voltages at least on the order of 500 mV, as indicated by good reproducibility and lack of opening of the curve at lesser voltages. Many workers have reported corrosion as low as 350 mV, so that these powders seem more stable in acid than typical industrial grade powder. Steady-state polarization curves for both WC NBS and WC 165 are compared in Figure 11. The ratio in activities is 1.1 at 50 mV and 1.9 at 200 mV.

One might immediately be surprised by the similarity of the two curves when the large differences in the hydrogen chemisorption are remembered. This question will be addressed in a later section. Clues to understanding this are available from the spectroscopic surface studies.

Typical potentiodynamic curves produced for the titanium carbide system are shown in Fig. 12. The magnitudes of current densities in either case are extremely small. Curve shapes and rest potentials were found to depend greatly on the history of the electrode. Rest potentials exhibited very slow recovery times and usually had values greater than 100 mV, sometimes 500 mV. This is a mixed potential, with hydrogen oxidation not having an exchange current measurable in this experiment for any of these materials. The purest carbides had the lowest rest

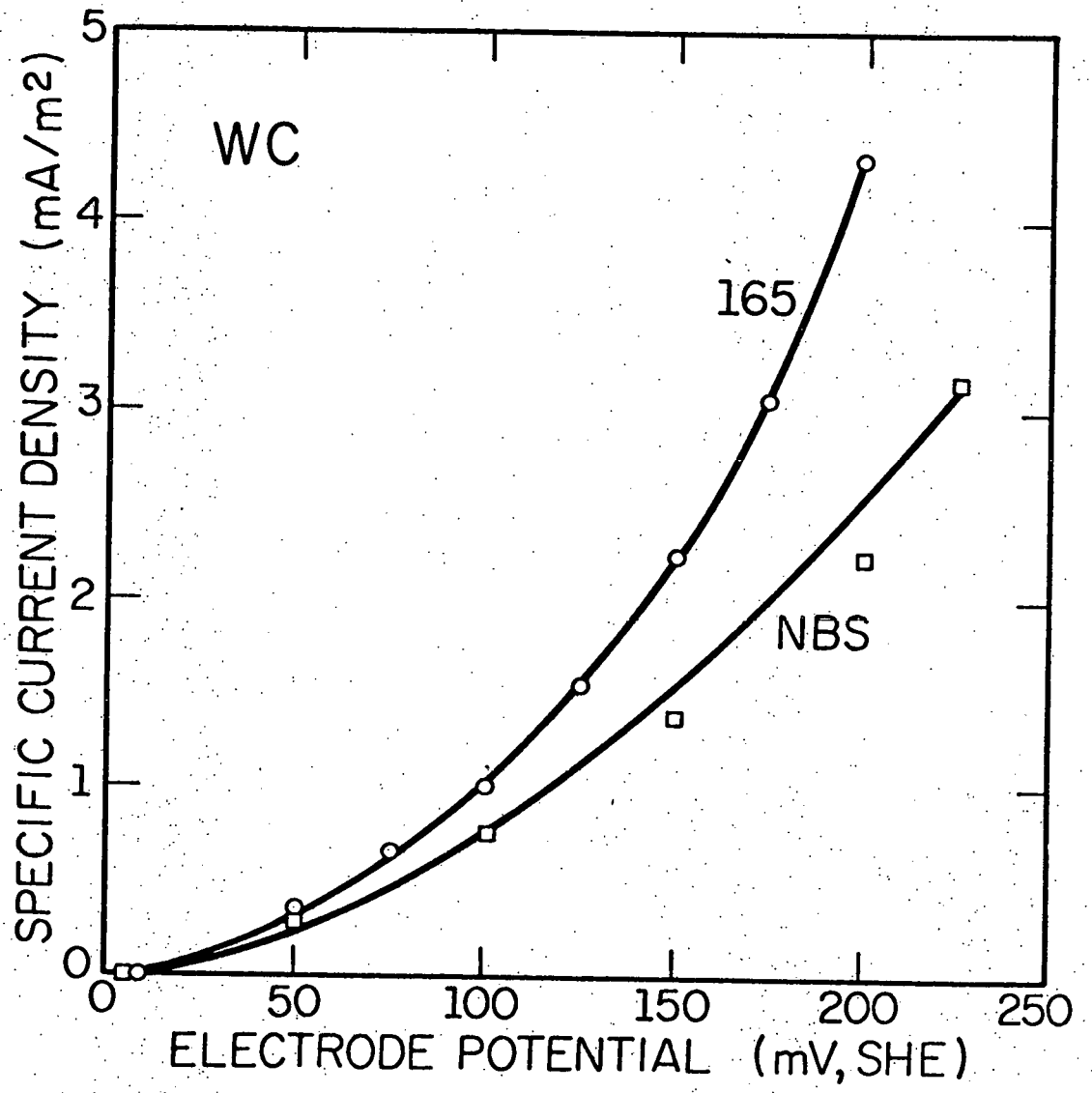

Figure 11. Hydrogen oxidation polarization curves for WC NBS, WC 165, 1N H_2SO_4, 22°C, 1 atm. H_2.

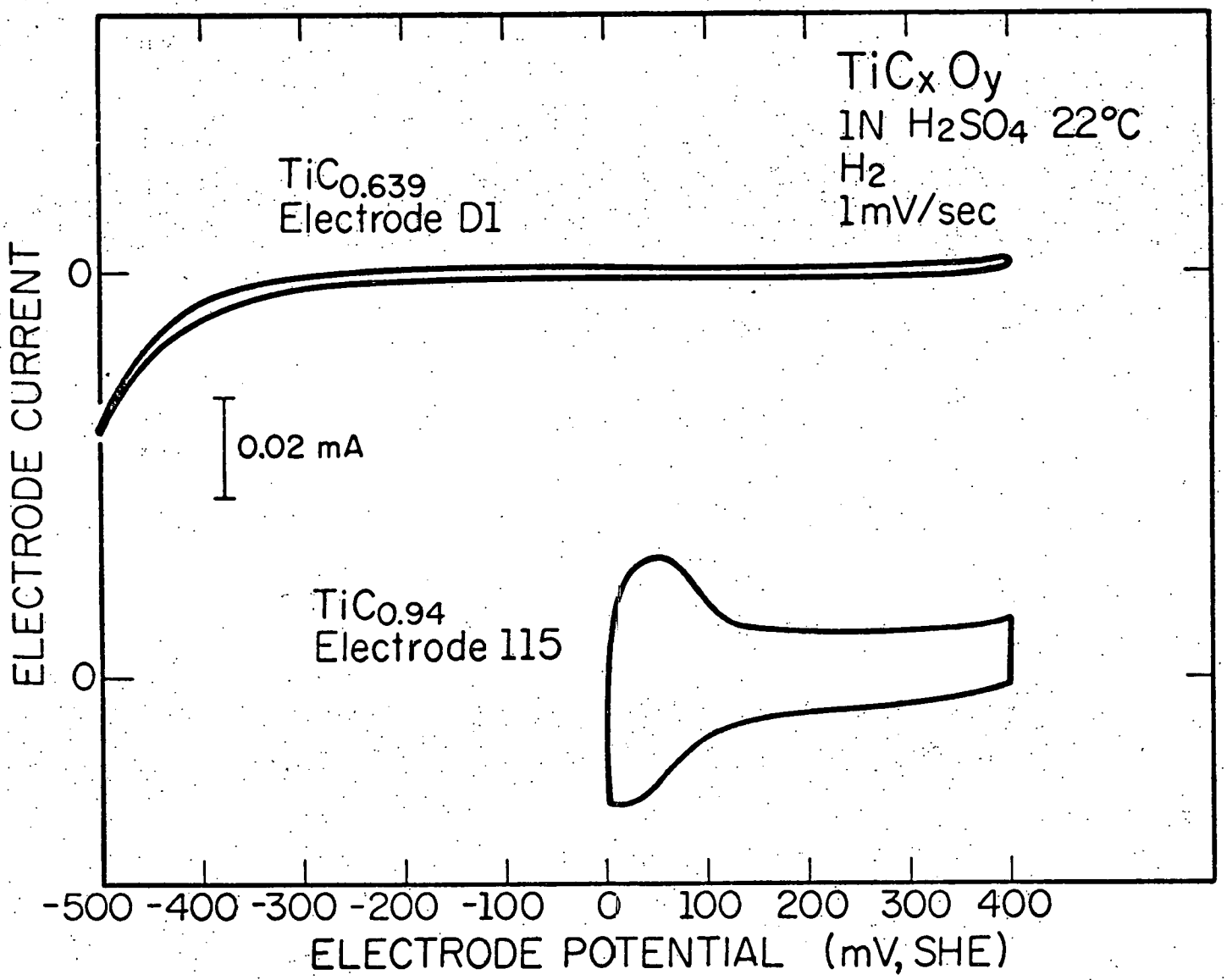

Figure 12. Typical potentiodynamic curves for TiC_x.

potentials however. This could be due to the Fe^{+3}/Fe^{+2} reaction, for example (see Table 1). Several electrodes were dipped in HF and measured a second time. This generally lowered E_o for the least pure powders and left the other unaffected, and agrees with impurities accounting for at least part of the variation of E_o from 0 V. The curve for $TiC_{.94}$ (electrode 115) exhibits typical features for this type of material. The flat opened region of the curve from E_o to 500-700 mV is due to charging of the double layer and is related to the real surface area of the powders that is exposed. A slight current rise at the high voltage end is the beginning of corrosion. The hump near 0 V was not found for all powders. Also, it appeared only when starting the scan from 0 V, indicating the reversible oxidation of some species in limited quantity. The lower branch of the curve is its reduction. This might in fact be due to a very small amount of hydrogen adsorbed at 0 V. It should be noted separately here that WC/TiC 70/30 behaved in much the same way, that is, it was found inactive.

A more careful study of any subtle effects of substitutional oxygen and carbon vacancies in titanium carbide could not be made with these powders and this technique of making electrodes. The materials exhibit very low specific current densities and slow drift of rest potentials. In addition, for this type of teflon-bonded electrode it is very hard to bond such large particles together to provide structural integrity and hydrophobic properties without on the other hand covering the particles with teflon. The effect of this is shown by the curve for $TiC_{.64}$ (electrode D2). The effective area of the electrode is very low, as seen by the thinness of the charging region. Any possible small differences in the behavior of the various TiC_xO_y compositions were masked by this problem. However, it may be concluded that point defects do not significantly enhance the activity of these cubic carbides.

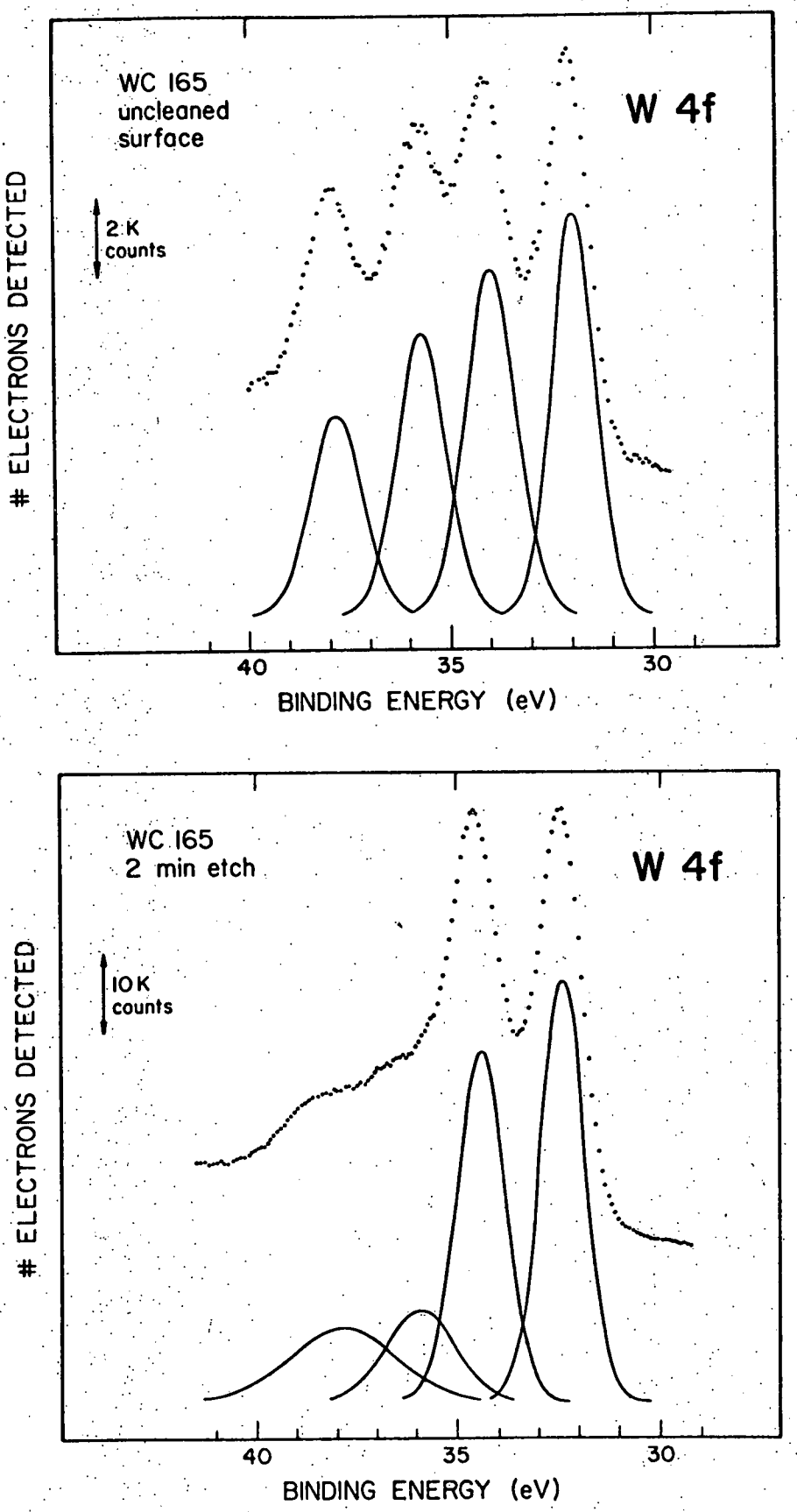

Figure 13. ESCA W4f spectra, uncleaned and etched WC 165 surfaces. See Note 3, Table 5.

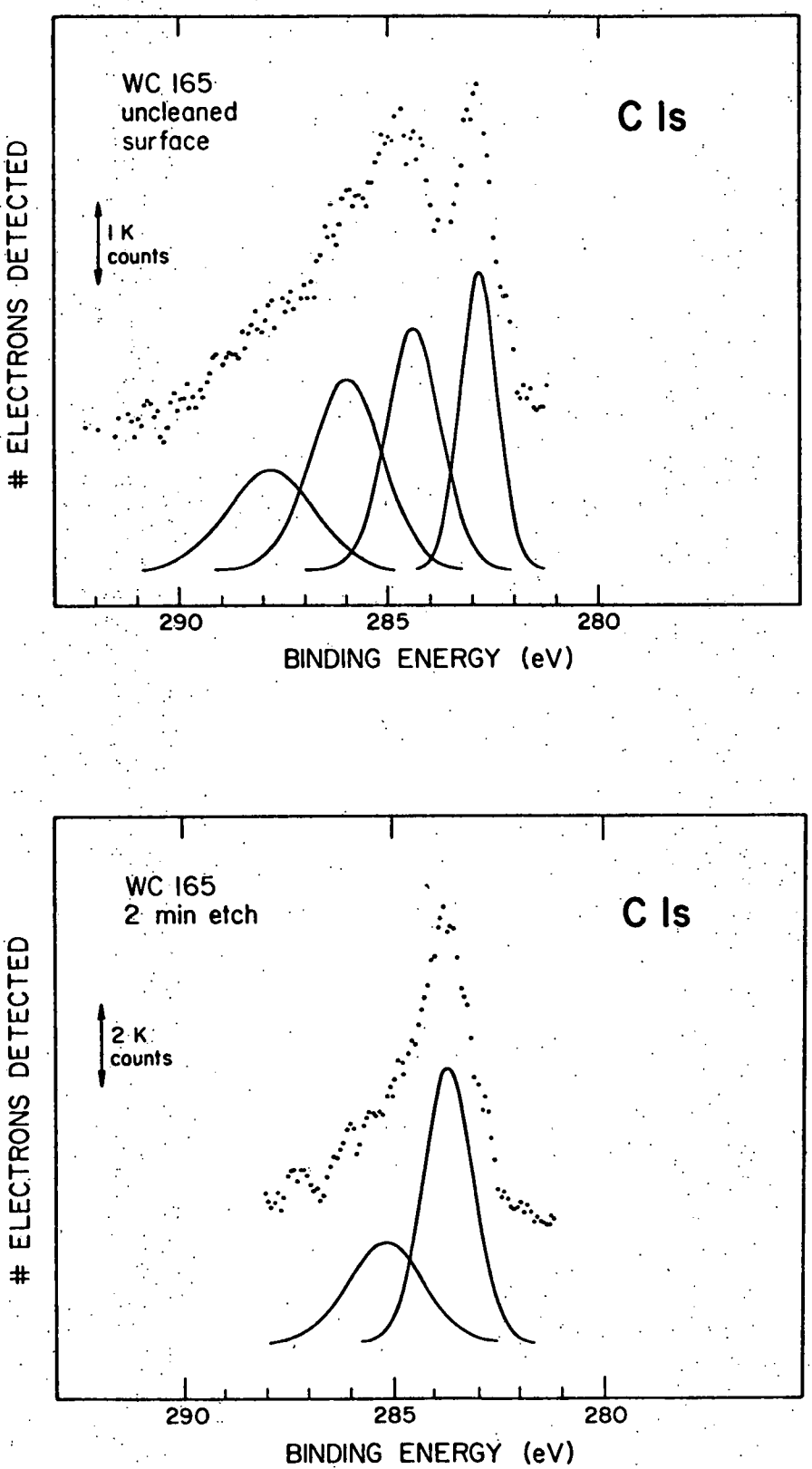

Figure 14. ESCA Cls spectra, uncleaned and etched WC 165 surfaces. See Note 3, Table 5.

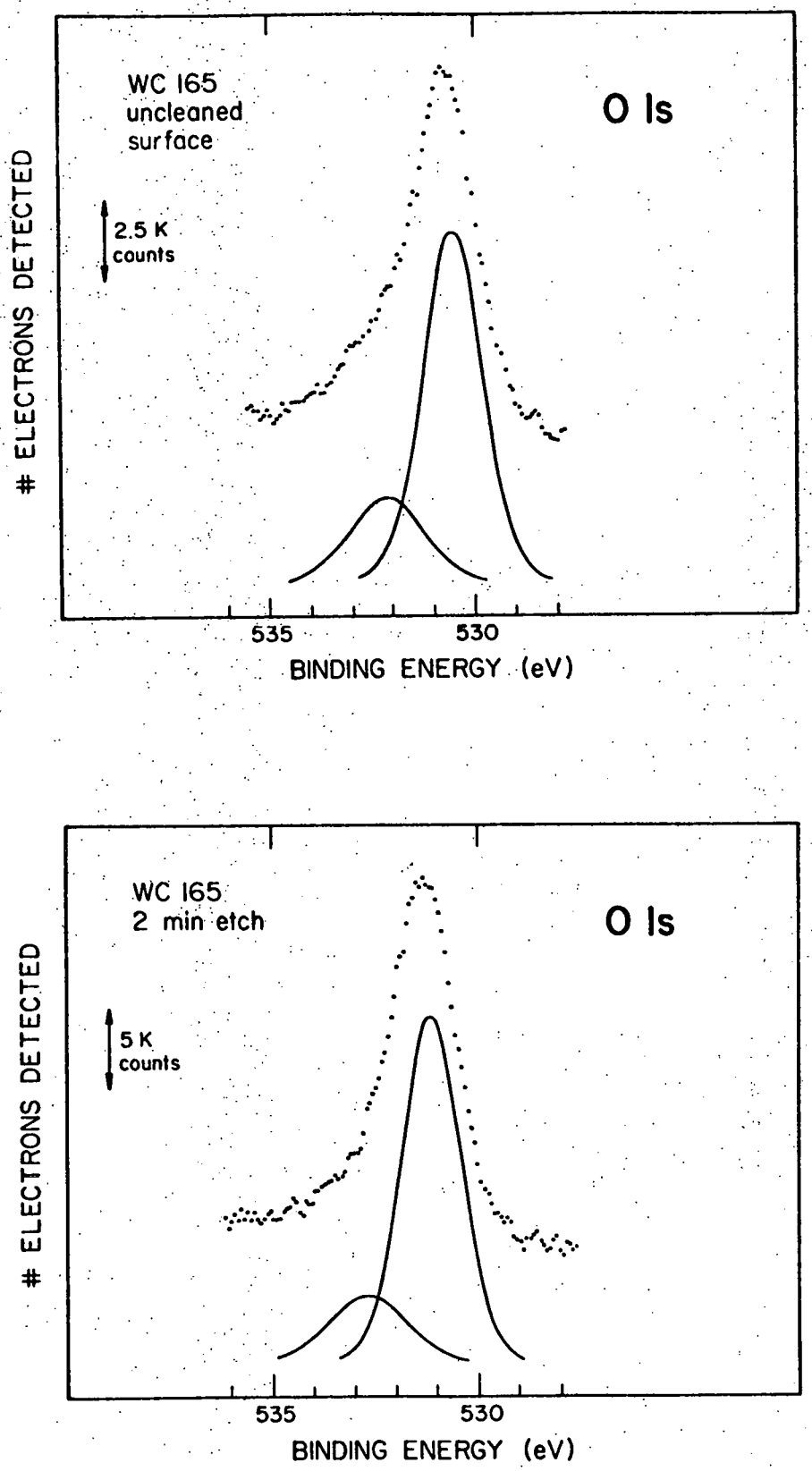

Figure 15. ESCA O1s spectra, uncleaned and etched WC 165 surfaces. See Note 3, Table 5.

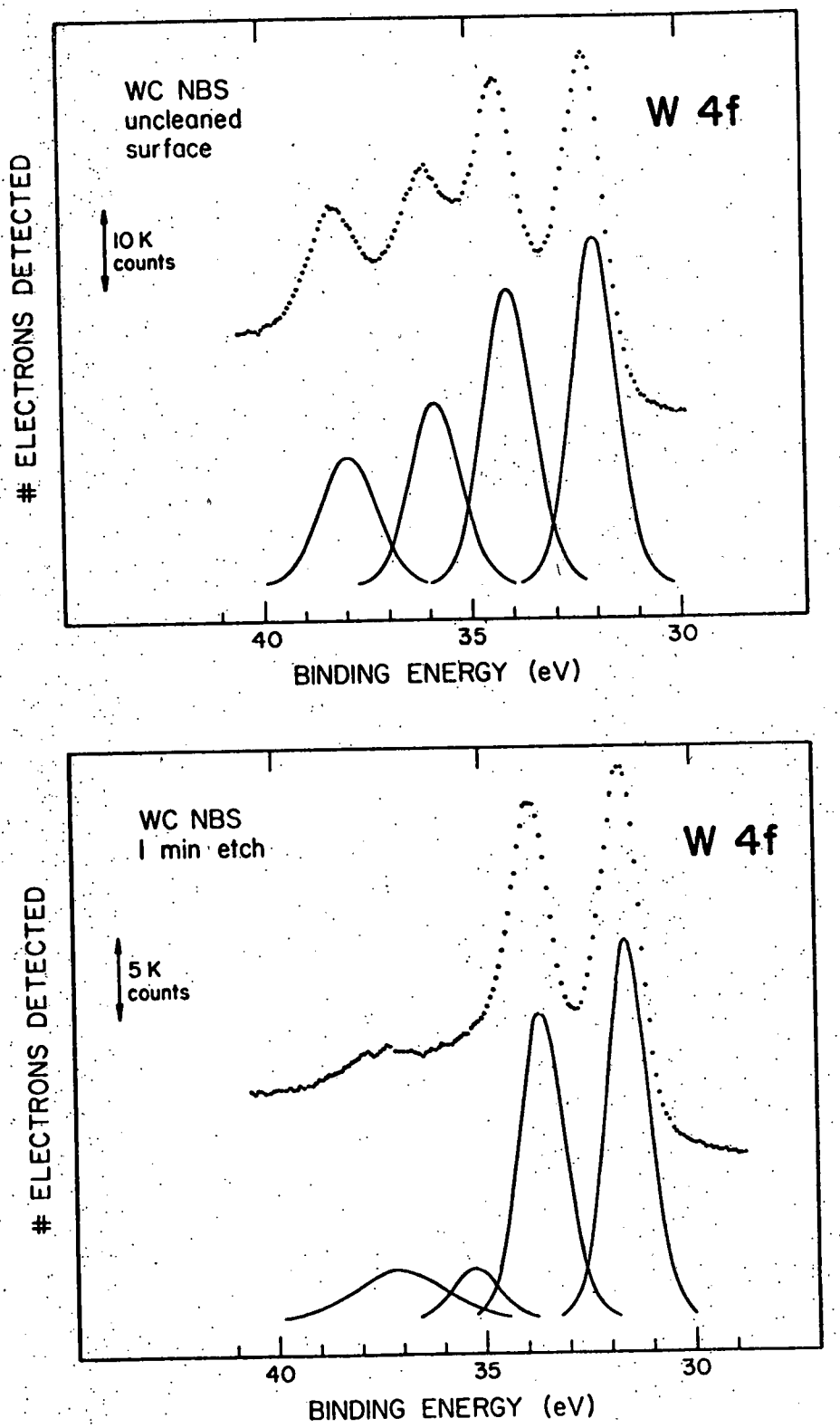

Figure 16. ESCA W4f spectra, uncleaned and etched WC NBS surfaces.

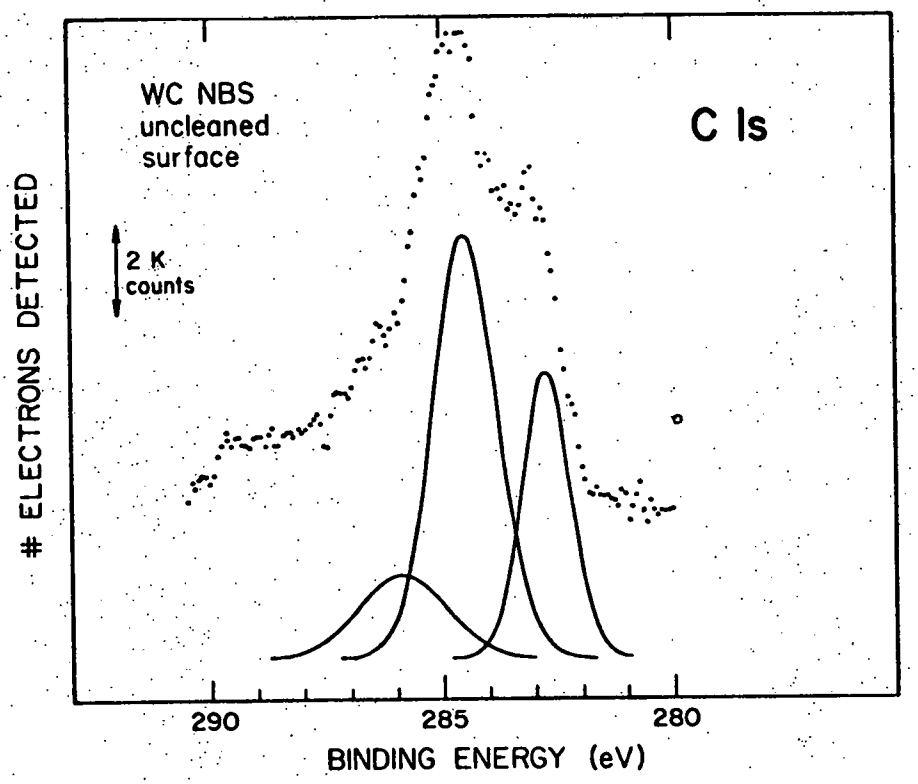

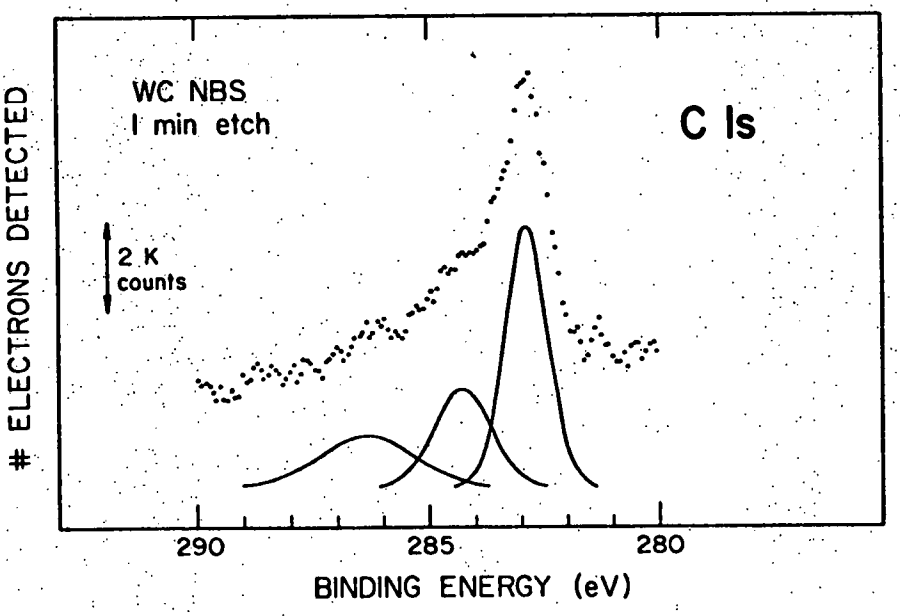

Figure 17. ESCA Cls spectra, uncleaned and etched WC NBS surfaces.

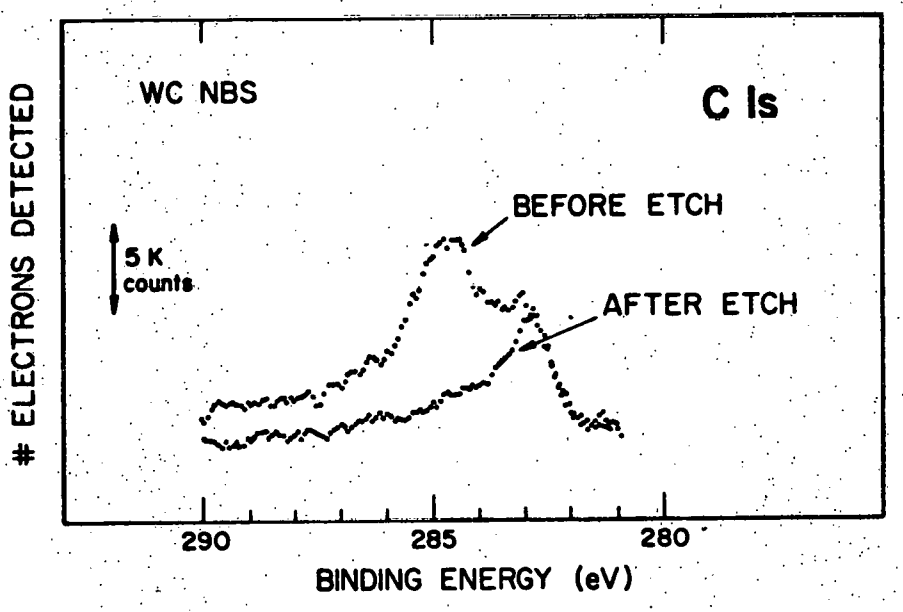

Figure 18. ESCA C1s spectra on WC NBS. Before and after etch compared.

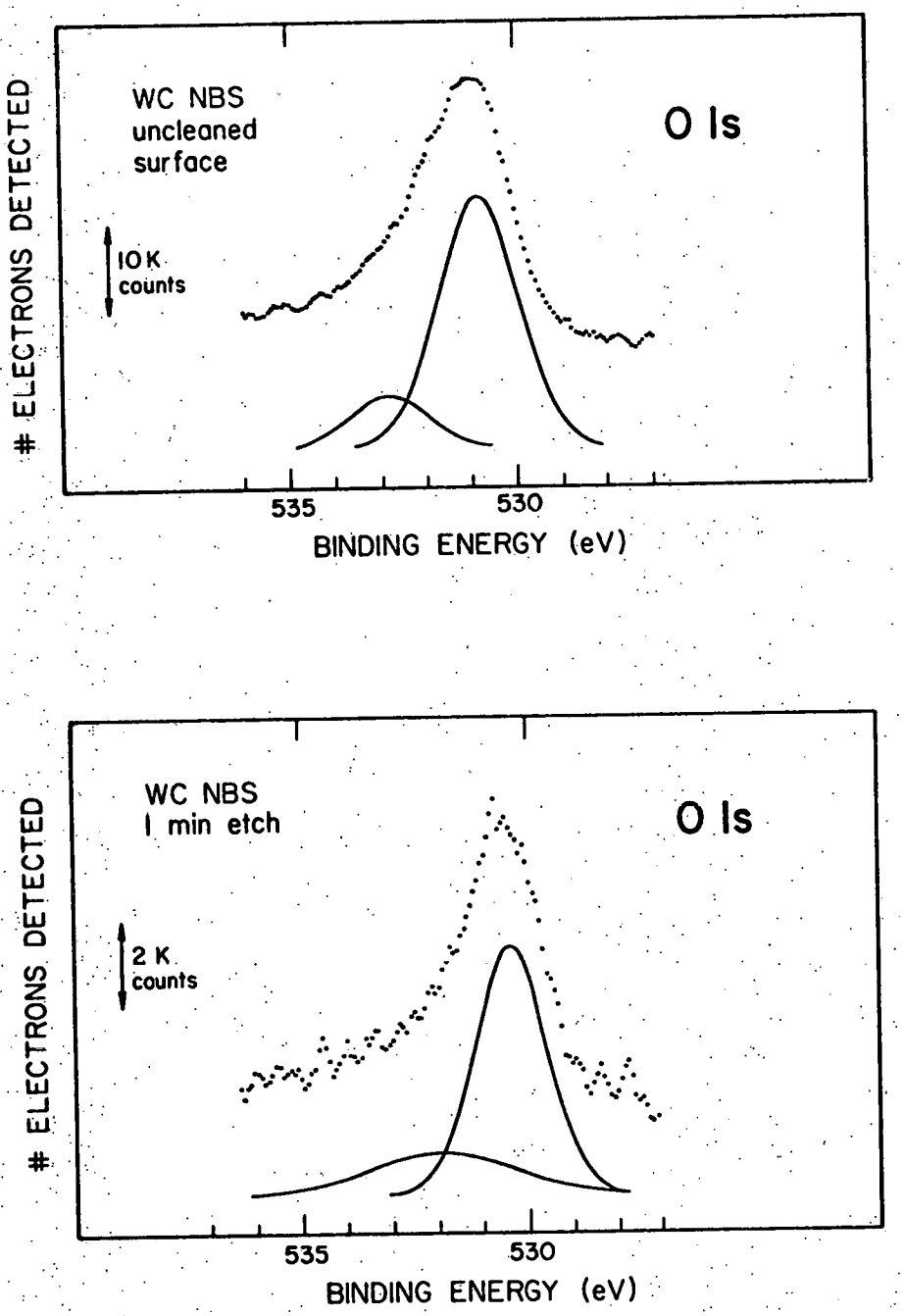

Figure 19. ESCA O1s spectra, uncleaned and etched WC NBS surfaces.

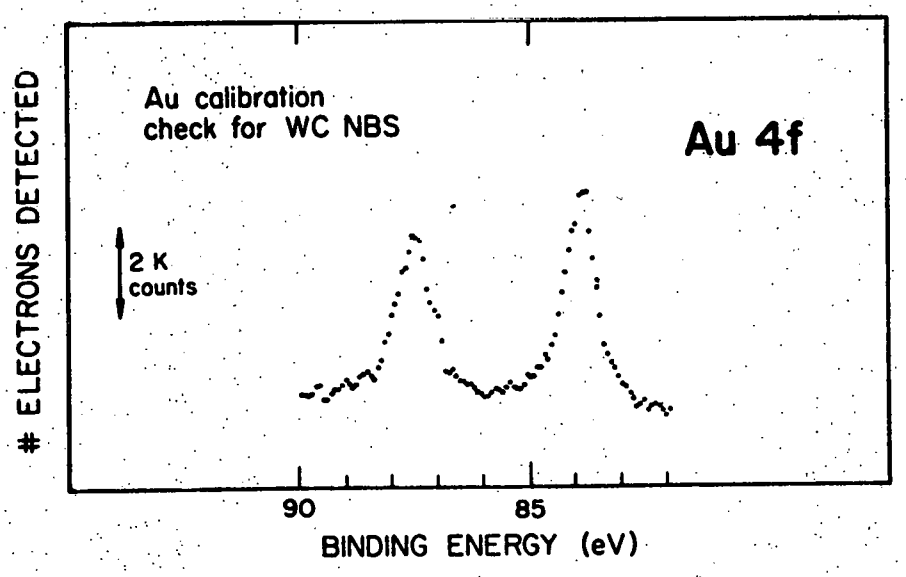

Figure 20. ESCA spectrometer calibration check using Au4f at 83.8 eV.

D. Surface Studies

1. X-Ray Photoemission

In their study of tungsten carbide catalysts, Ross and Stonehart [19] were unable to examine the carbon ESCA signal because of carbon contamination inside their spectrometer and did not look at the oxygen spectra. Neither did they sputter clean or sputter profile the surface. Carbon deficiency will be important to look at—it was already speculated earlier in this study that the low carbon content of the WC 165 may be due to WO_3 pockets. Also separation of the spectra into chemical states at the surface is a critical aspect of this work.

Figures 13-19 plot the W 4f, C 1s, and O 1s regions before and after a brief etching and Tables 5 and 6 condense data from these plots and list the results of compositional calculations. Binding energies in Tables 5 and 6 were corrected by calibration with Au 4f (Fig. 20). Although the sputtering rates for W, C, and O are unknown for tungsten carbide, on silica the etch times with the same conditions would correspond to depths of 7 Å (1 min. etch), 14 Å (2 min. etch), 105 Å (15 min.), and 0.16 μ (40 min.). WC however sputters much more slowly than does SiO_2, so this is a maximum estimate of depth. The first 1 or 2 min. of etch should be only a surface dusting or cleaning and will remove most weakly bound contaminants. The W 4f region consists of two sets of 4f doublets arising from two distinct chemical states. The $4f_{7/2}$-$4f_{5/2}$ doublet at low binding energy can be identified as carbide W lines; this doublet is the chemical state W I in Tables 5 and 6. The second $4f_{7/2}$-$4f_{5/2}$ doublet is higher in binding energy by 3.8 eV, compared to tabulated value of 4.1 eV for the difference between WO_3 and WC, so that W II of Tables 5 and 6 should be assigned to W in WO_3. The lowest binding energy singlet C 1s peak (C I) is unaffected by short sputtering times and is assigned to the carbide C. This is seen graphically in Fig. 18. The other three peaks that appear in Fig. 14 appear to be singlets that disappear on long sputtering. A contamination peak at 284.4 eV is commonly observed.[48] Increasing the

apparent oxidation number as we go to higher binding energy we may try very simple mindedly to assign C II as carbon in C-C bonds, C III as C-O-C or =COH groups, C IV as C=0 groups. Since we have assigned W II to WO_3 and there is only one major oxygen peak it would be most sensible to assign O I to O in WO_3. One would expect a second small O peak to be associated, at least partly, with the hydrocarbons from the carbon peak. Sayers and Armstrong [48] observe two O 1s peaks on several varieties of titanium oxides, all having the same values, 520.1 eV and 531.7 eV, with the second peak assigned to O from adsorbed water. From Table 5, the difference in binding energies between O I and O II is exactly the same as for these materials. So it seems to be most likely from ESCA that the major states at the surface involve a large degree of WO_3 with the tungsten carbide. For WC 165 this confirms the idea from bulk combustion analysis that WO_3 is a large percentage of the bulk.

To examine the surface of the tungsten carbides more closely, we remove the contributions from the contamination peaks and recalculate the surface composition. Results are shown in column (b) of Table 5. If we assume that WO_3 and WC_x are the two phases present in this clean surface, we find that the surface composition by phase is 0.5 (WO_3) + 0.5 ($WC_{.81}$). This must only be a surface phase since as we move into the bulk the composition measured by combustion analysis must be found. More will be said about using the ESCA sputtering data later. Doing this same analysis for WC NBS, one finds that the surface exists as 0.4 (WO_3) + 0.6 ($WC_{.8}$). In the case of the NBS powder the oxide phase, however, is located only in a very thin layer of the surface (compare Figs. 15 and 18). An additional difference in the two uncleaned surfaces is seen in Figs. 14 and 17. C II (284.5 eV) was assigned to C-C bonds, that is, free carbon on the surface. This is usually more tenacious than the hydrocarbons which we've assigned to peaks C III and C IV. For WC 165 (Fig. 14)

Table 5. Surface compositions and binding energies from ESCA[4] data for WC 165 (Ar^+ beam, $V_{acc.}$ = 3 kV, $I_{emis.}$ = 15 mA).

Chemical state	Composition (atom %) Bulk[1]	Before etch[2] (a)	(b)	2 min. etch[3]	15 min. etch	40 min. etch	BE (corrected) (eV) Before etch	2 min. etch	Δ(2 min. etch)
W I		12.6	(20.)	29.3	~39.	~47.	32.30	31.80	0.5($4f_{7/2}$)
II		8.9	(14.)	11.3	~ 9.	~ 9.	35.98	~35.22	0.8($4f_{7/2}$)
Total	42.9	21.5	(34.)	40.6	47.8	55.7			
C I		8.9	(14.)	18.6	*	*	283.13	283.13	---
II		10.4	-----	10.3	----	----	284.69	284.64	---
III		10.8	-----	----	----	----	286.28	------	
IV		7.0	-----	----	----	----	288.13	------	
Total	36.8	37.1	(14.)	28.9	27.3	21.9			
O I		32.4	(52.)	24.4	*	*	530.57	530.58	---
II		9.1	-----	6.1	----	----	532.14	532.15	
Total	20.3	41.5	(52.)	30.5	25.0	22.3			

*Composition not separated into individual states because of decreasing resolution.

[1]From combustion analysis for carbon and oxygen.

[2]Column (a) lists compositions from data by individual state. Column (b) lists compositions after removing contribution estimated for the surface contamination film.

[3]Performed at a later date on fresh sample.

[4]These studies were performed by Surface Science Laboratories, Palo Alto, CA.

Table 6. Surface compositions and binding energies from ESCA[2] data for WC NBS (Ar^+ beam, $V_{acc.}$ = 3 kV, $I_{emis.}$ = 15 mA)

Chemical state	Composition (atom %) Bulk[1]	Before etch	1 min. etch	BE (corrected) (eV) Before etch	2 min. etch	Δ(1 min. etch)
W I		15.7	35.9	32.10	31.61	0.5 ($4f_{7/2}$)
II		8.6	7.8	35.95	35.33	0.6 ($4f_{7/2}$)
Total	48.7	24.3	43.7			
C I		11.6	21.4	282.86	282.84	----
II		22.7	10.4	284.57	284.25	0.3
III		5.9	9.1	285.99	285.32	0.7
Total	50.3	28.6	40.9			
O I		29.7	11.4	530.89	530.44	0.4
II		5.9	3.8	532.86	531.93	0.9
Total	1.03	35.6	15.2			

[1]From combustion analysis for carbon and oxygen.

[2]These studies were performed by Surface Science Laboratories, Palo Alto, CA.

free carbon is the only non-carbide species remaining on the surface. The surface of WC NBS (Fig. 17) is seen to have a much larger concentration of free carbon on the surface. In addition, a third species (BE = 285.3 eV) is retained on the surface after a 1 min. etch. Its nature has not been understood in this study. It is possible, however, that a further 1 min. etch would remove this species.

Thus, the picture we are building is of a carbon-deficient tungsten carbide phase stabilized by the close mixing of a WO_3 phase, or perhaps even by some amount of oxygen substitution. WC 165 has a surface relatively clean of free carbon. The surface of the NBS powder is covered more heavily with free carbon, but otherwise, has a very similar composition. We propose that the discrepancy noted previously between the chemisorption and hydrogen behavior of these two powders is due to different coatings of free carbon on the surface. In the case of WC 165 the powder was active for both gas-phase and liquid-phase reactions. WC NBS, however, was only able to chemisorb hydrogen when in acid electrolyte. We suggest that this surface with carbon vacancies as sites is activated by removal of free carbon in acid electrolyte. The active surface is clean of free-carbon and has the composition 0.5 (WO_3) + 0.5 ($WC_{.8}$). Some additional oxygen substitution into the carbide phase may be required to stabilize this structure.

It should be pointed out that there is another way to have a carbon-deficient surface and that is have selected planes from the WC crystal structure exposed. It is known that tungsten carbide in the hexagonal phase has polar character of crystal faces of the $(10\bar{1}0)$ type.[50] These expose all metal or all carbon surfaces. A preferential exposure of these planes could also give the tungsten-rich surfaces found above by ESCA. We believe, however, that these faces would adsorb oxygen too strongly to allow this explanation to account for the observed catalytic activity of tungsten carbide.

One word of clarification about the Ar^+ ion etching is needed. The major purpose of the sputtering data was to identify certain species as belonging only to the surface, and to make relative qualitative assessments between WC NBS and WC 165 of the structure of the particles from surface inward. One should not expect quantitative data from a heavily sputtered surface containing atoms of widely different masses and chemical states. This is due to preferential sputtering (see Auger section of this study). This manifests itself for metal-oxide surfaces through the metal ion reduction by the ion beam, with the resulting shift in the photoemission state populations [49] of the metal. If one examines the prolonged sputtering of WC 165 (Table 5) one sees a continuous increase in W concentration and loss of both C and O due to differential sputtering in both WO_3 and WC_x (part of the relative loss of oxygen may be due to sputtering through the oxide-rich layer). The total W a/o increases, mainly in the W I state. This probably creates an amorphous tungsten-rich state.

A comparison of these results with ideas from the theoretical models will be made in last section of this chapter.

2. Auger Electron Spectroscopy

It was decided to test the ability of AES to give a quantitative description of carbide surfaces and to examine more closely the preferential sputtering of the carbides by the Ar^+ ion beam.

Figures 21 and 22 show the Auger spectra after brief ion cleaning for the two most widely differing samples studied in the TiC_xO_y system. Characteristic differential signals for C (272-254 eV), Ti (451-330 eV) and O (510-475 eV) are seen, together with a sulfur surface impurity on $TiC_{.400}O_{.455}$ (Fig. 22). One can also notice the change in shape in the Ti signal of this last spectrum. This is called a "chemical effect" on the Auger peaks, and is due to the influence of the large amounts of oxygen in the lattice.

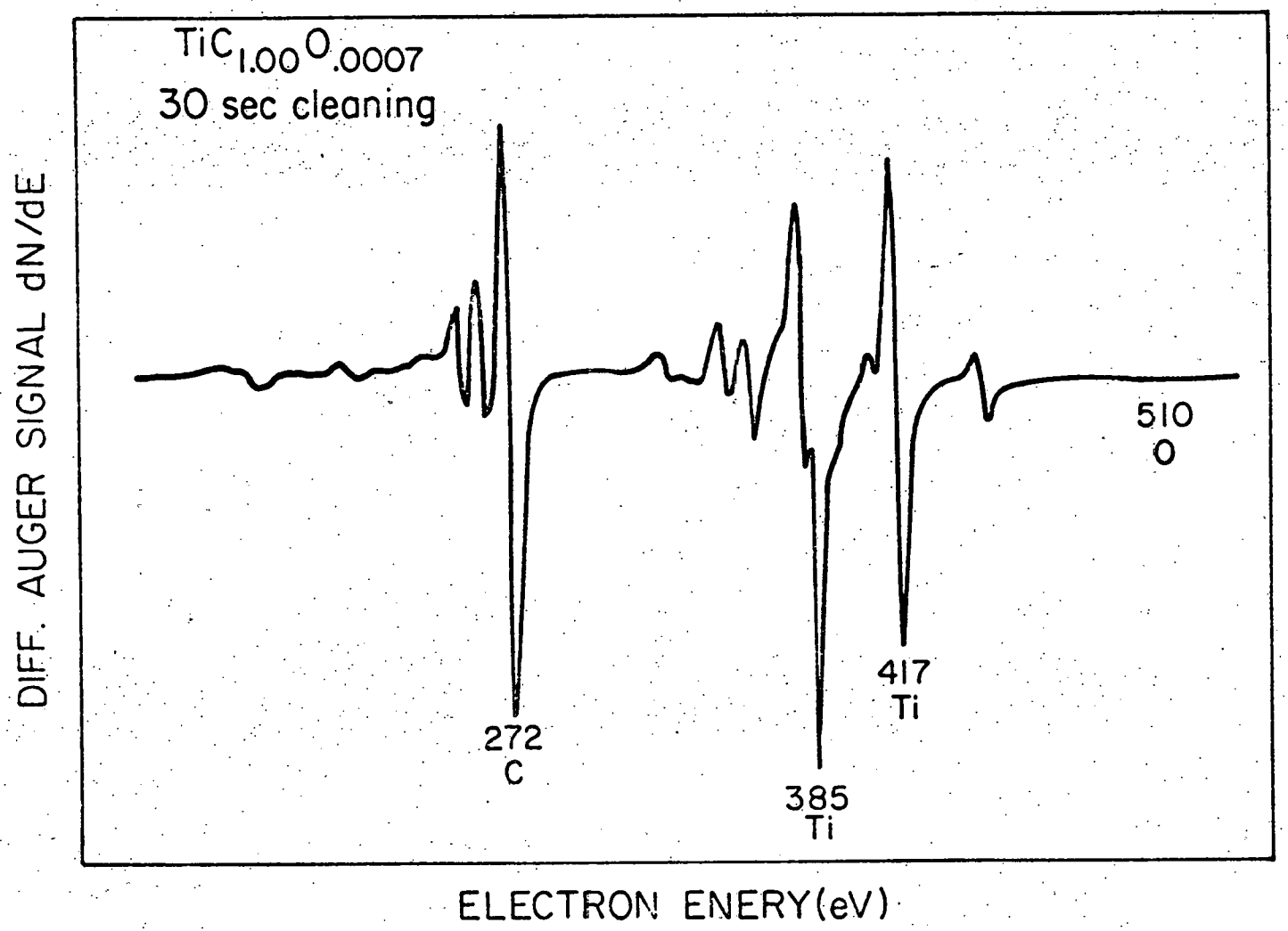

Figure 21. AES spectrum for $TiC_{1.00}O_{.0007}$.

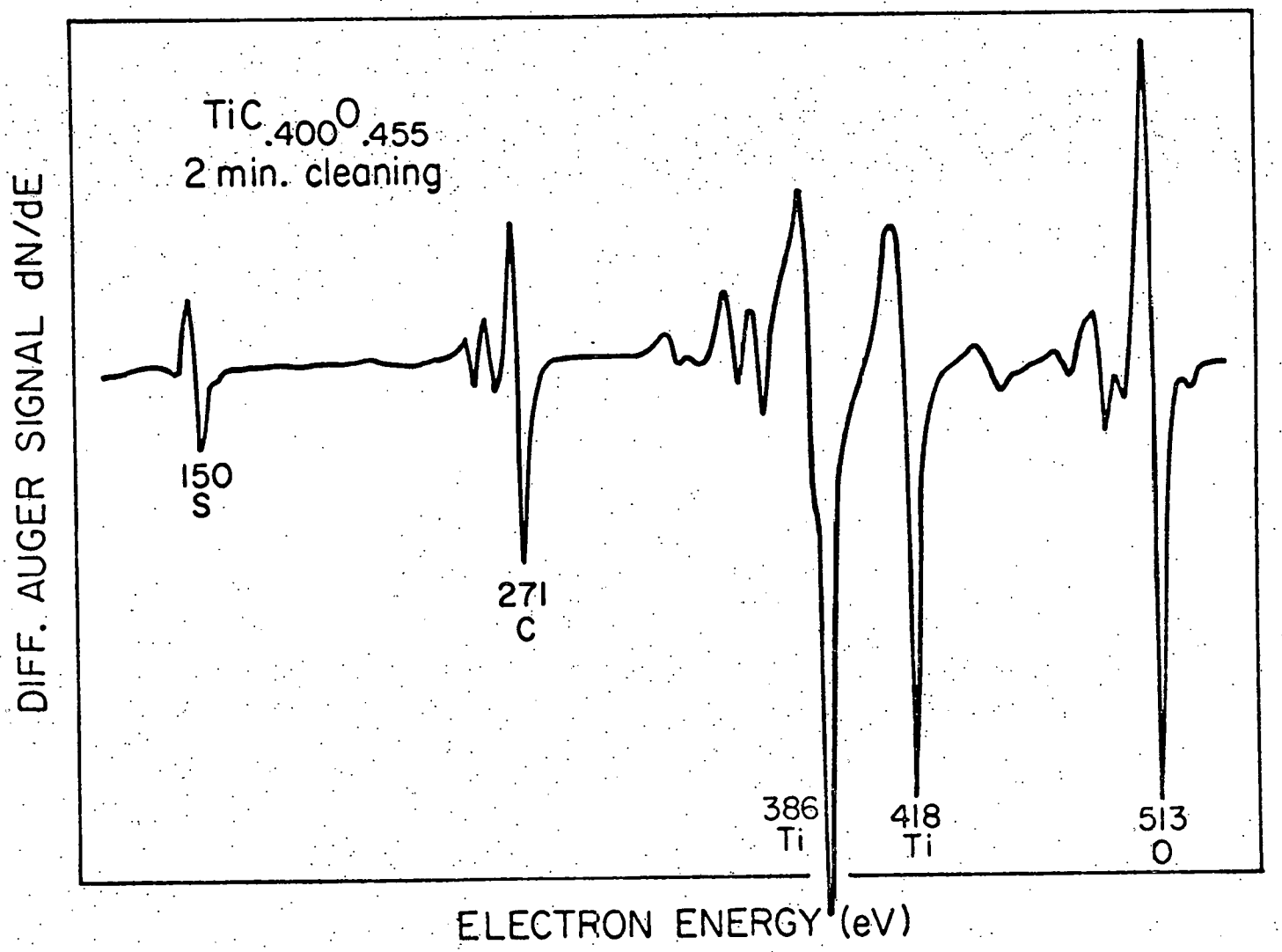

Figure 22. AES spectrum for $TiC_{.400}O_{.450}$.

Although semiquantitative methods are available for surface analysis by Auger spectroscopy [51] the best results are still obtained by preparation of standards. In this case, an entire system with three variable components is available. The major problems facing this study, it was felt, were the reproducibility of the instrument differential sputtering, and the nature of the samples themselves. It was not known whether the surface of a material containing a large number of vacancies in the bulk would retain this characteristic at the surface.

The distinctive, symmetric shape of the carbon peaks in the carbides is well known.[52] This characteristic shape can be used to distinguish a surface covered with free carbon or hydrocarbons from the clean carbide surface. To make a quantitative measurement of the surface C/Me ratio, however, this free carbon must be removed. In this work, the shape of the C spectra was monitored to allow an optimum sputtering time to be chosen that would also avoid the effects of preferential sputtering seen also in the ESCA studies.

Figure 23 shows the results found for sputtering materials in the TiC_xO_y system. The two vertical axes are compositions found from Auger data in a way to be described later. It was found that at about 2-3 min. sputtering with the previously described conditions, the carbon peaks assumed a nearly perfect carbide shape and retained that for the remainder of the sputtering. After this time the sputtering behavior of TiC_xO_y materials divided these materials into two classes. For materials where $x + y < 1$, it was found that the proportion of C increased relative to Ti. For the more stoichiometric compositions ($x + y \approx 1$) the C composition remained the same over very long sputtering times. In both cases the O composition decreased until some equilibrium value was reached at sputtering times much greater than 2 min. This could be caused by either migration of carbon atoms to the surface or preferential removal of Ti atoms.

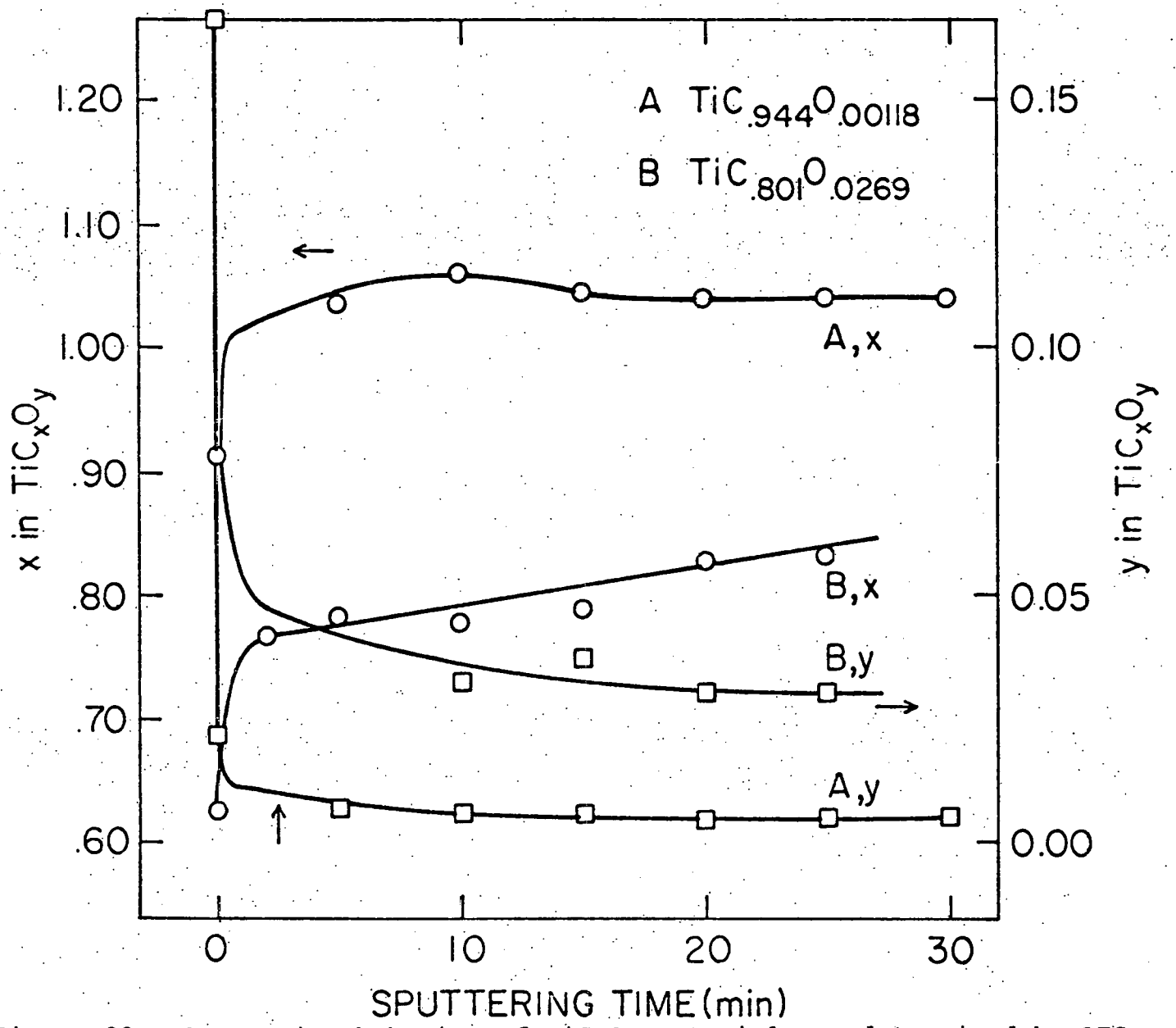

Figure 23. Sputtering behavior of TiC_xO_y materials as determined by AES.

Since it is not believed that the effect of beam heating of the sample would be enough to overcome the high migration energy of carbon atoms,[53] it is believed that Ti atoms are differentially removed from the surfaces of the defective materials. This coincides with the vaporization behavior of these materials, where Ti atoms are volatized at high temperatures, causing the materials to approach stoichiometry during long firing times. It should be appreciated that current theories normally treat differential sputtering as a mass-related phenomenon, predicting the reverse behavior in this system.

In the absence of "chemical effects" on the shapes of Auger spectra, the normal method of determining surface compositions from AES is to measure peak-to-peak heights of the differential signals and normalize these heights to the height of one of the major constituents. For this study C and O ptp heights were normalized to both the Ti 418 ptp height and the Ti 384 ptp height. The results are plotted in Fig. 24 for carbon-to-metal ratio, and in Fig. 25 for oxygen-to-metal ratio. The resulting calibration equation for carbon-to-metal ratio was found to be:

$$x = .958 \frac{C}{Ti_{418}} - .182 \quad . \tag{4}$$

These compositions found from these calibration curves for a particular normalized Auger ratio is felt to represent the true surface composition even though x and y are found from bulk values. We believe this is true because of the large (4-5 eV/atom) activation energy for motion of C in the carbide.

The same calibration procedure when used for the Ti 384 peak produced the curve in Fig. 26. The reason for the inability of the Ti 384 peak normalization to correlate to composition is thought to lie in the interference of the energy loss processes from the Ti 418 peak with the structure of the Ti 384 peak. The primary electron beam was examined (Fig. 27) for a single crystal of TiC and found to exhibit major loss peaks at 18 and 45 eV below the main peak. These are probably due to plasmons.

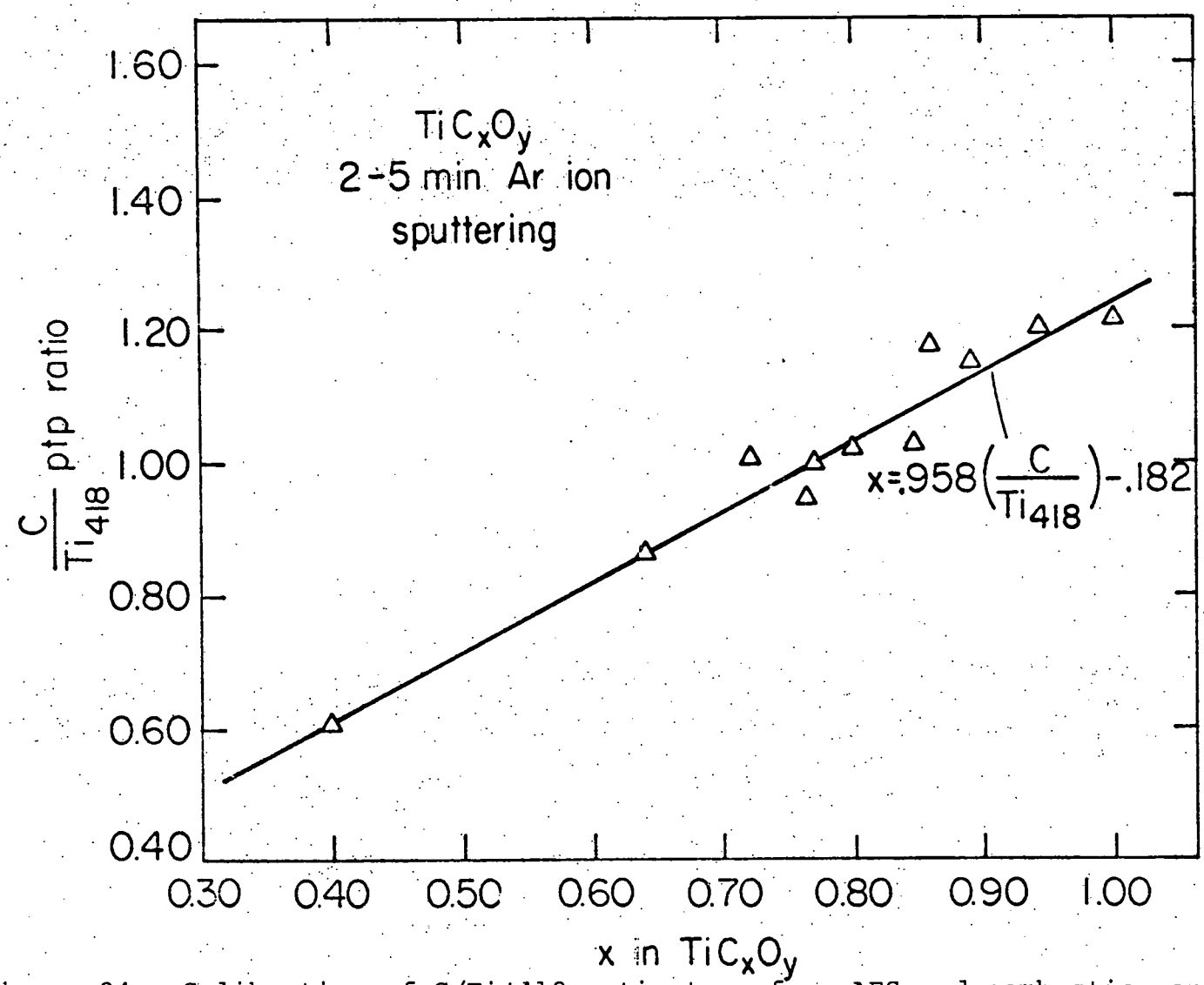

Figure 24. Calibration of C/Ti 418 ratio to x from AES and combustion analysis data.

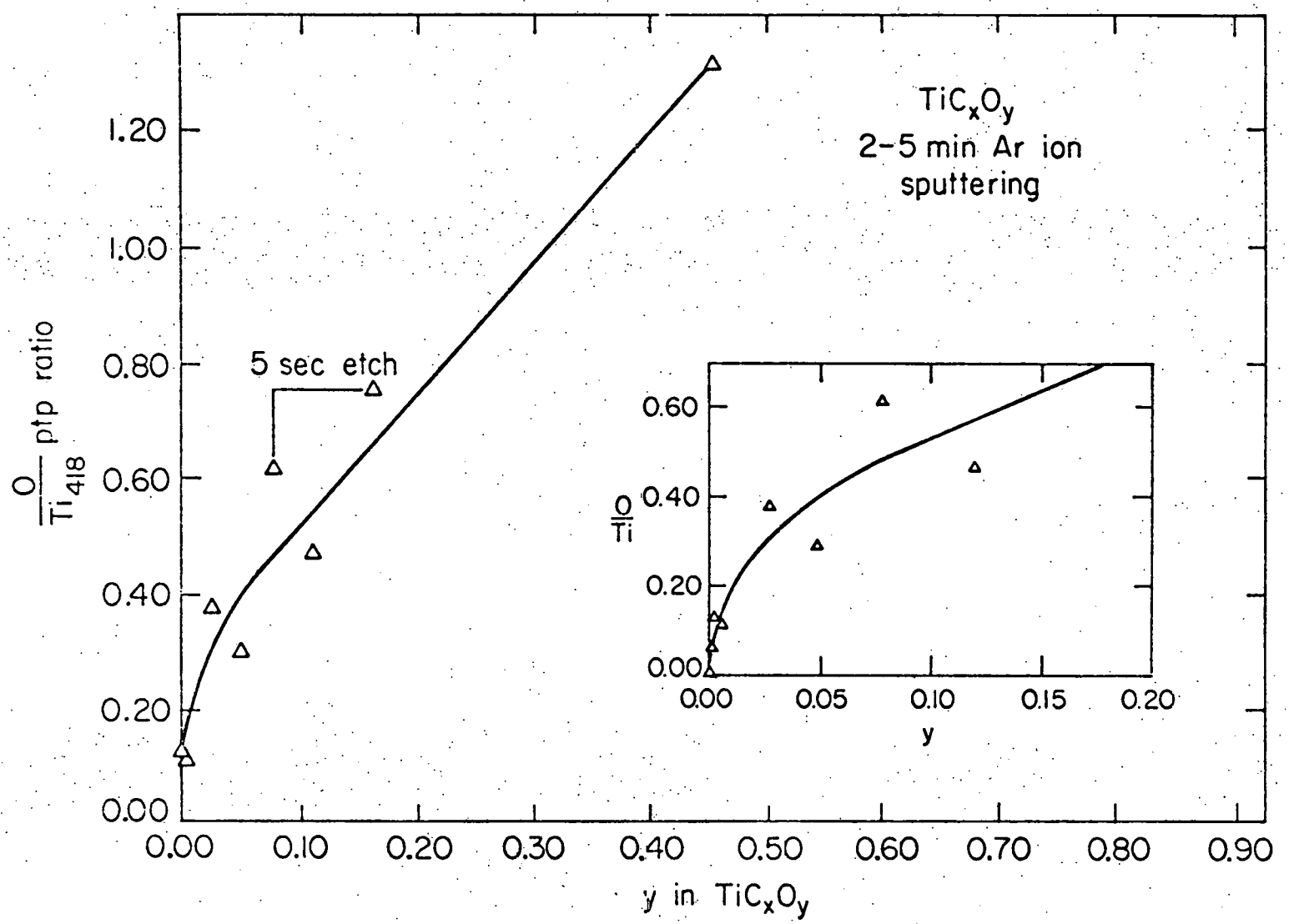

Figure 25. Calibration of O/Ti 418 ratio for y from AES and combustion analysis data

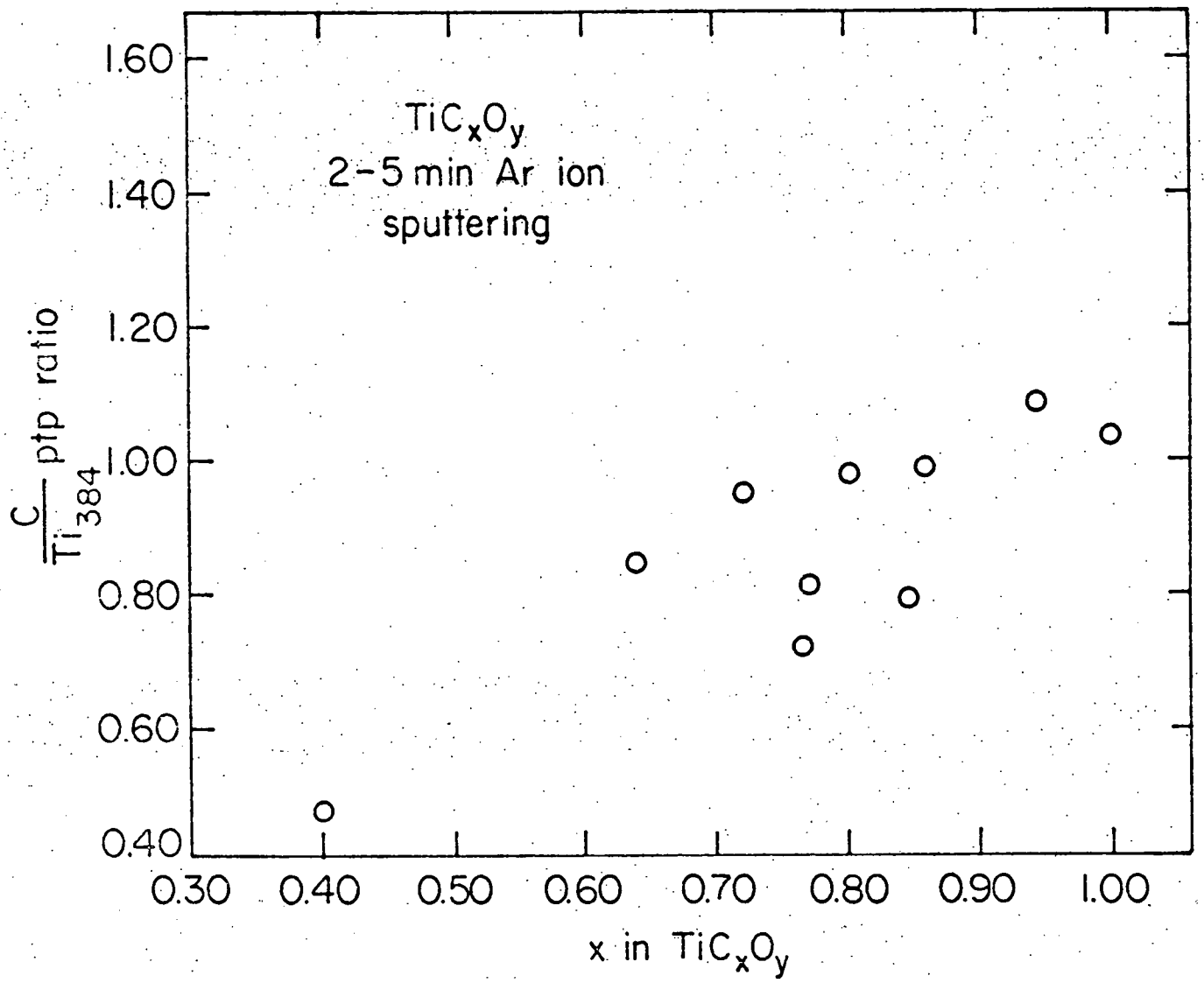

Figure 26. Calibration of C/Ti 384 ratio for x from AES and combustion analysis data.

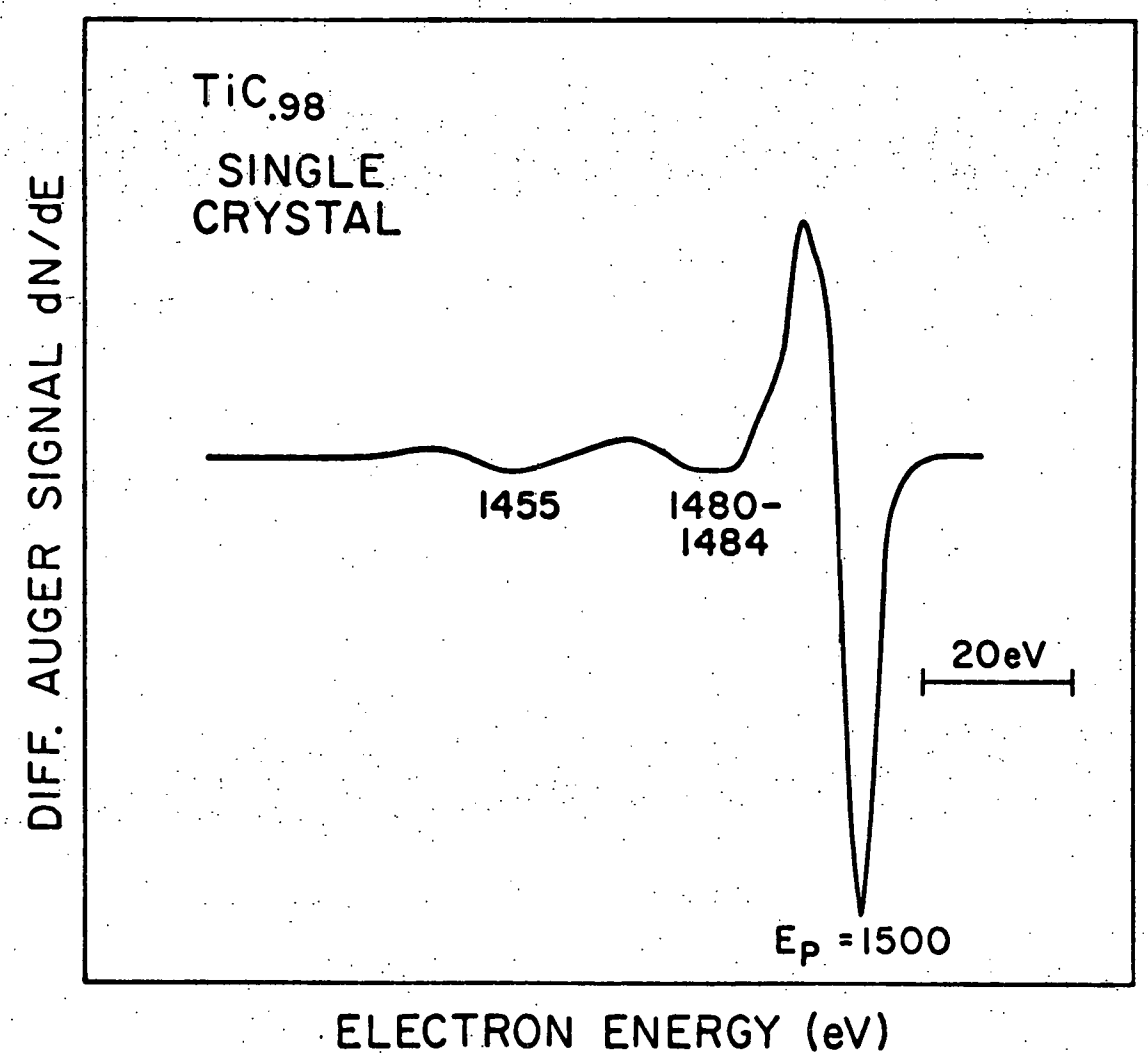

Figure 27. Electron loss processes from primary beam for $TiC_{.98}$ single crystal.

In addition, roughness effects from the powder specimens will allow further, inelastic processes to non-systematically scatter the data of Fig. 26.

Peak-to-peak heights cannot be used with these calibration curves to determine the amounts of C and O on a surface which is not ion cleaved. This is because of the shape change in the C spectra introduced by the contamination film on the surface. These shape changes are caused by the different distribution of electrons in C orbitals for different bonding. This problem is resolved by using the second integral of the differential Auger signal in place of the peak-to-peak height. The derivative signal and its first integral for a $TiC_{.816}$ single crystal is shown in Fig. 28. This was made with a sample Simpson's rule approximation on the MRL computer.

These calibration procedures, together with the use of integrated Auger intensities will allow the study of surface phenomena and structure for the TiC_xO_y system. Their use can be extended to study other systems where suitable range of compositions allowing calibration exist.

AES spectra for WC NBS and WC 165 are shown in Fig. 29. Well-formed peaks for carbon are evident at 272 eV. An actual analysis of composition by AES techniques was not done. This was because of a lack of reproducibility of the spectra the several times the attempt was made to measure the signals. It was not understood whether this was due to instrumental effects or sample preparation. It is not possible for this to be due to powder inhomogeneity since the electron beam size was much larger than powder particle size. It can be noted from these spectra, however, that after 2 min. sputtering, the NBS powder has a higher concentration of carbon than the WC 165 does after 5 min. of sputtering. The oxygen peak has diminished due to preferential sputtering as was found in the ESCA data.

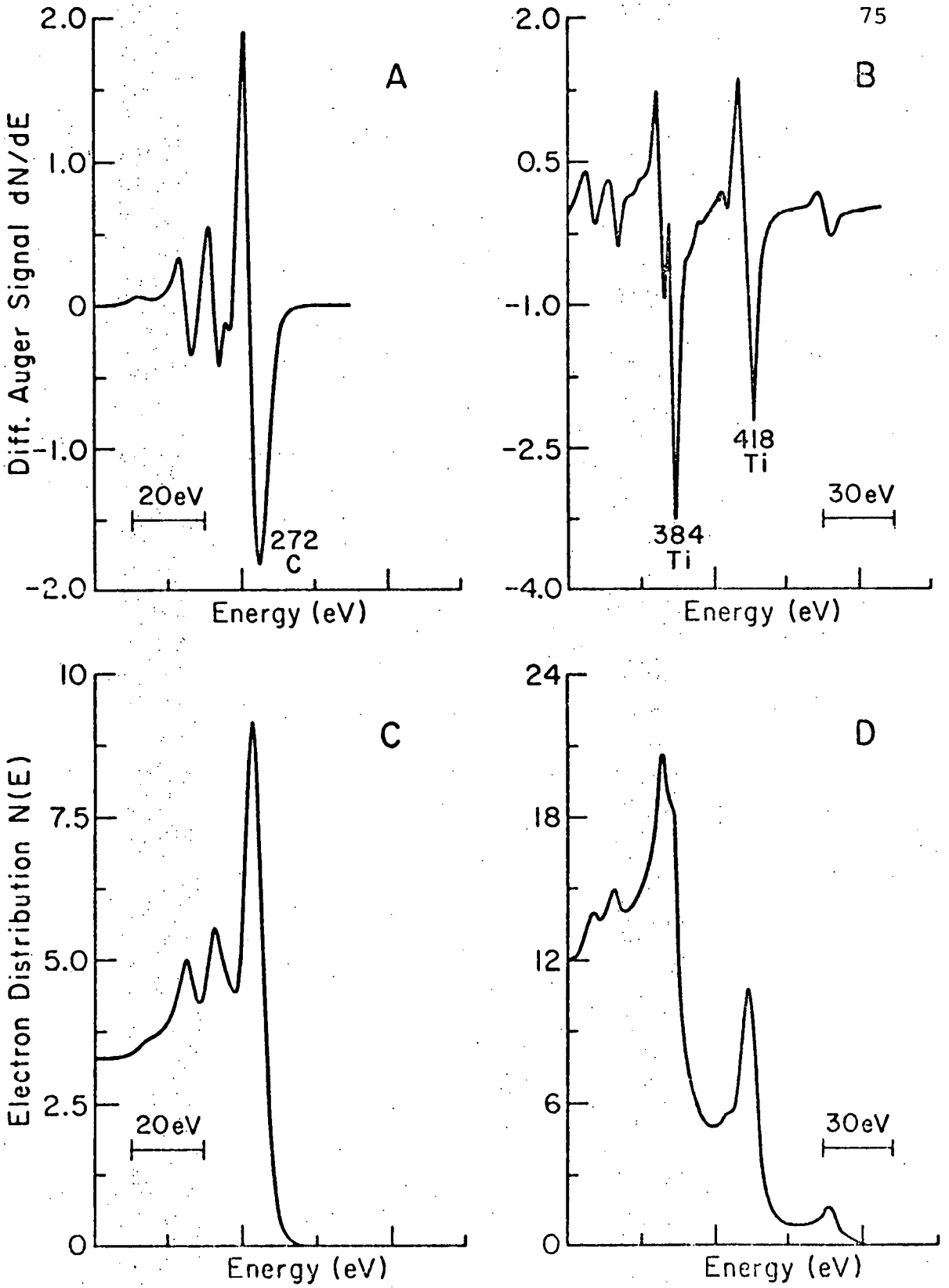

Figure 28. Derivative AES data and first integral curves for $TiC_{.816}$ single crystal.

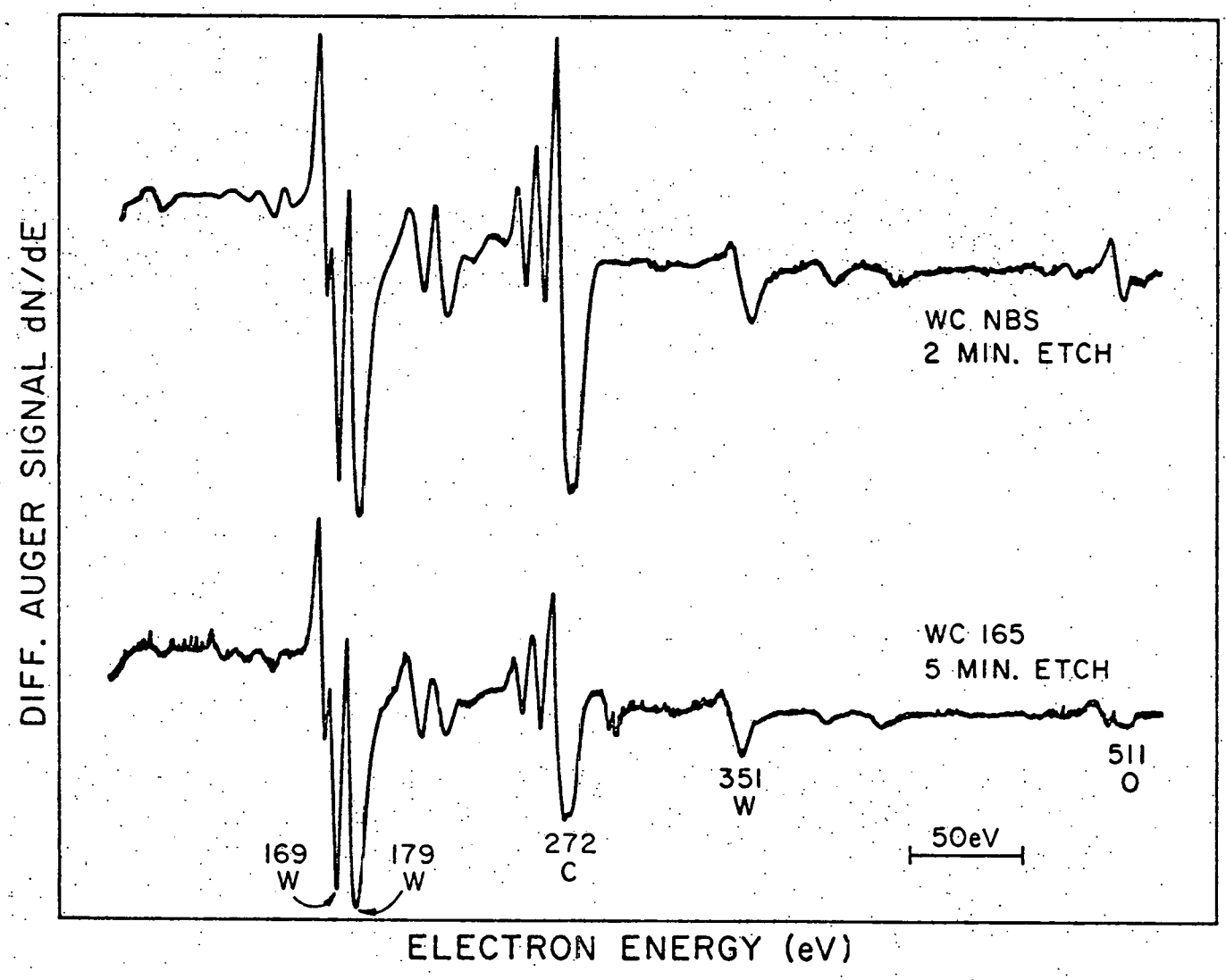

Figure 29. AES spectra for WC powders.

E. Electron Spin Resonance

The WC 165 powder was found to contain a large number of signals. Unfortunately it is believed that most of the signals are probably due to impurities with unpaired electrons (see Table 2). For example, the peak at g = 4.20 (G ≈ 1550) is due to Fe^{+3} in the rhombic symmetry--this is a well-known peak. Problems with the phase arm made it difficult to consistently make comparisons between ESR runs. However several observations were made:

1. WC NBS was very flat, except for a spike at g = 2.00, the free electron value, which was about 10G wide.
2. All narrow width peaks for WC 165 got larger with decreasing temperature (Fig. 30), whereas WC NBS appeared to get smaller.
3. A broad wave was observed in WC 165. This may be an instrumental effect or a surface effect with microwaves, due to high surface area. It shrinks and becomes distorted at 99°K.
4. Etching WC 165 with warm concentrated HCl decreased the size of the broad wave and the iron peak (Fig. 31). Most of the structure or the high g (low G) side of the free electron peak at 2.00 disappeared. However, a modified A peak (Fig. 32) (g = 2.06) remains and a peak at B (g = 1.90) grew larger. B was sometimes different on different runs. This might be associated with a surface adsorption.

This work was not extended beyond these observations. It was not felt that we would be able to separate the individual contributions to these curves. No signals from this work were identified as belonging to the O^- ion.

F. Relation to Theory

The role of active sites for catalysis has been emphasized by much of the new work in the field, and cluster calculations have helped to describe these sites.

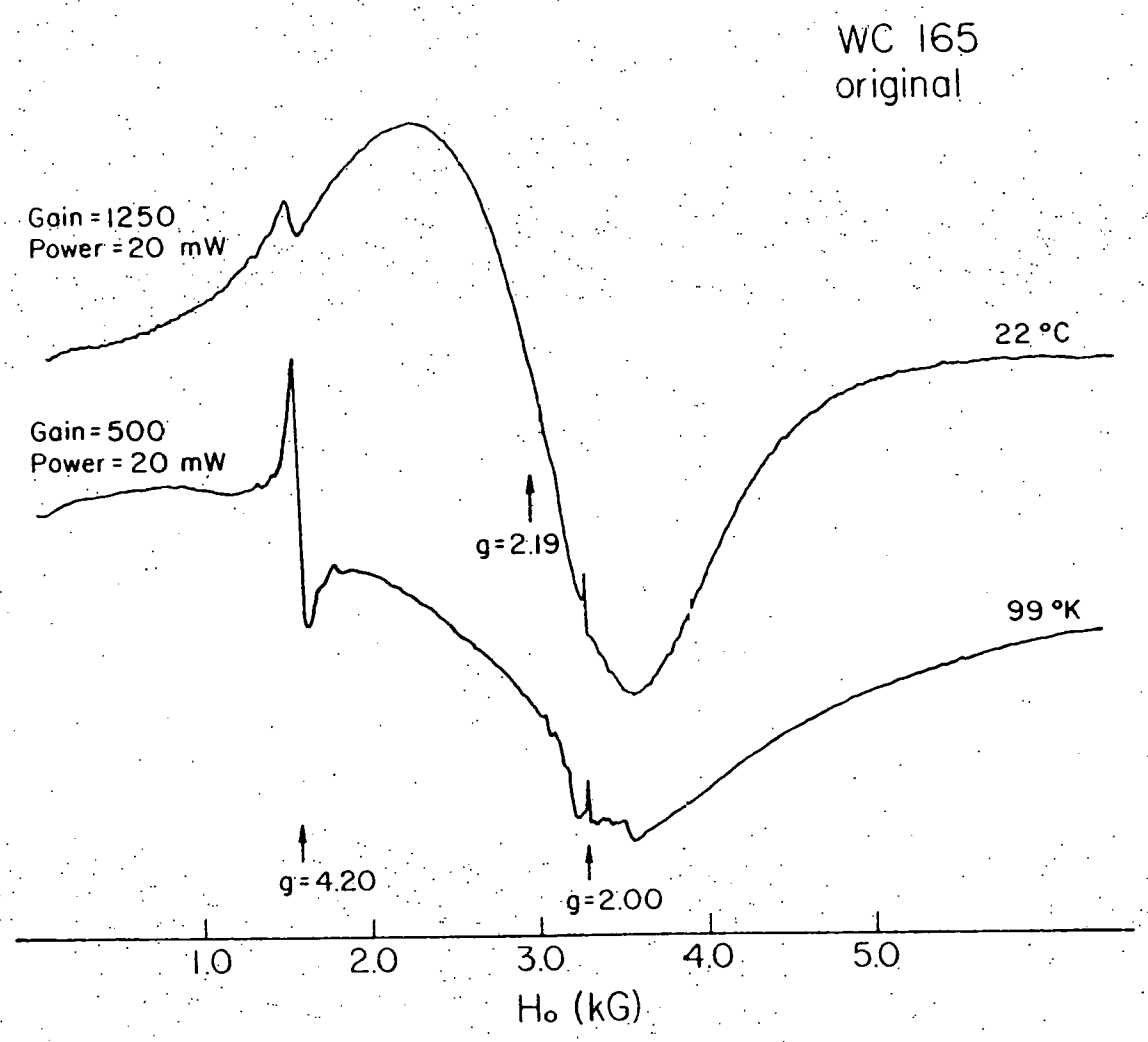

Figure 30. ESR spectra for original WC 165, 99°K, and 22°C.

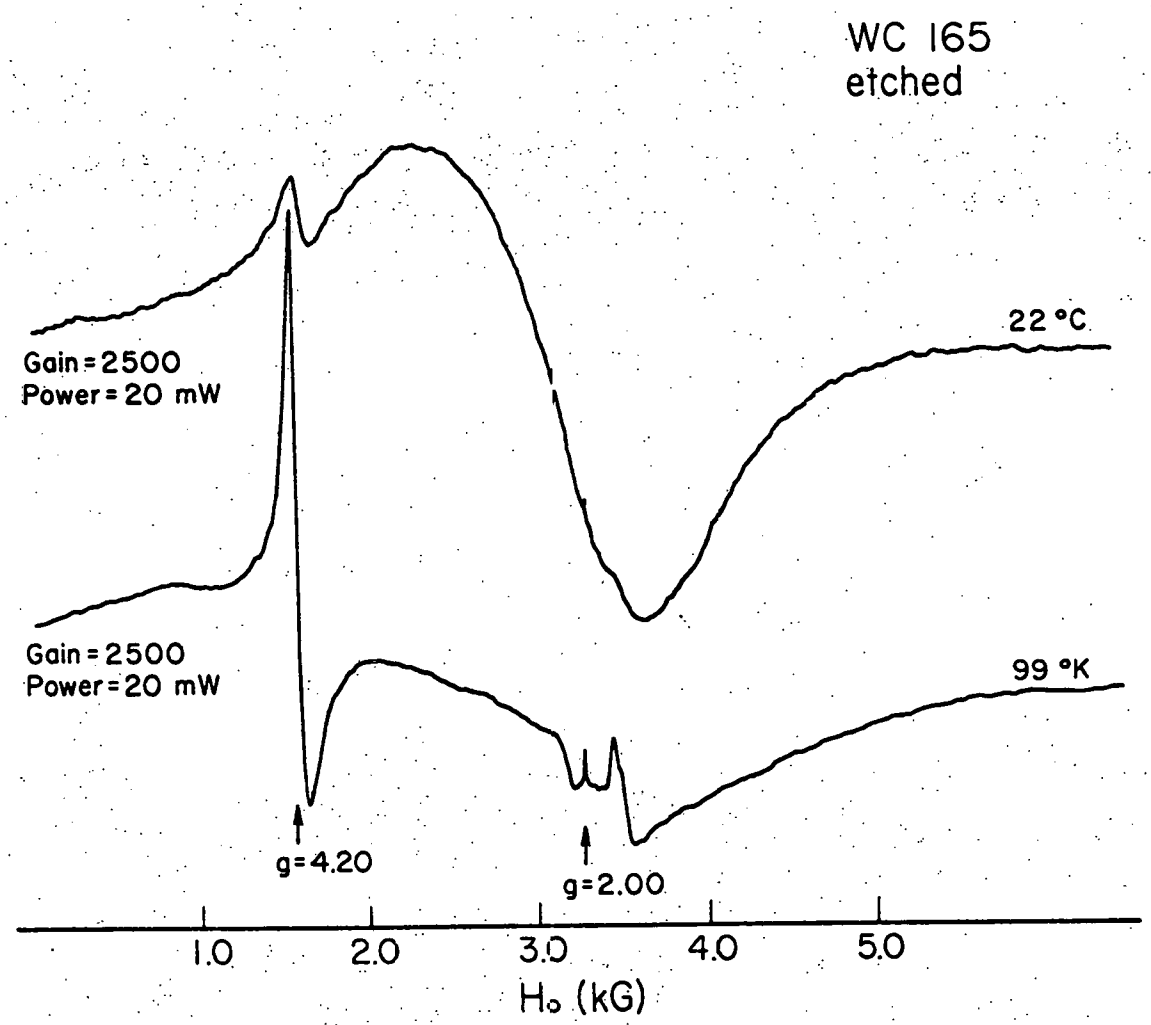

Figure 31. ESR spectra for etched WC 165, 99°K and 22°C.

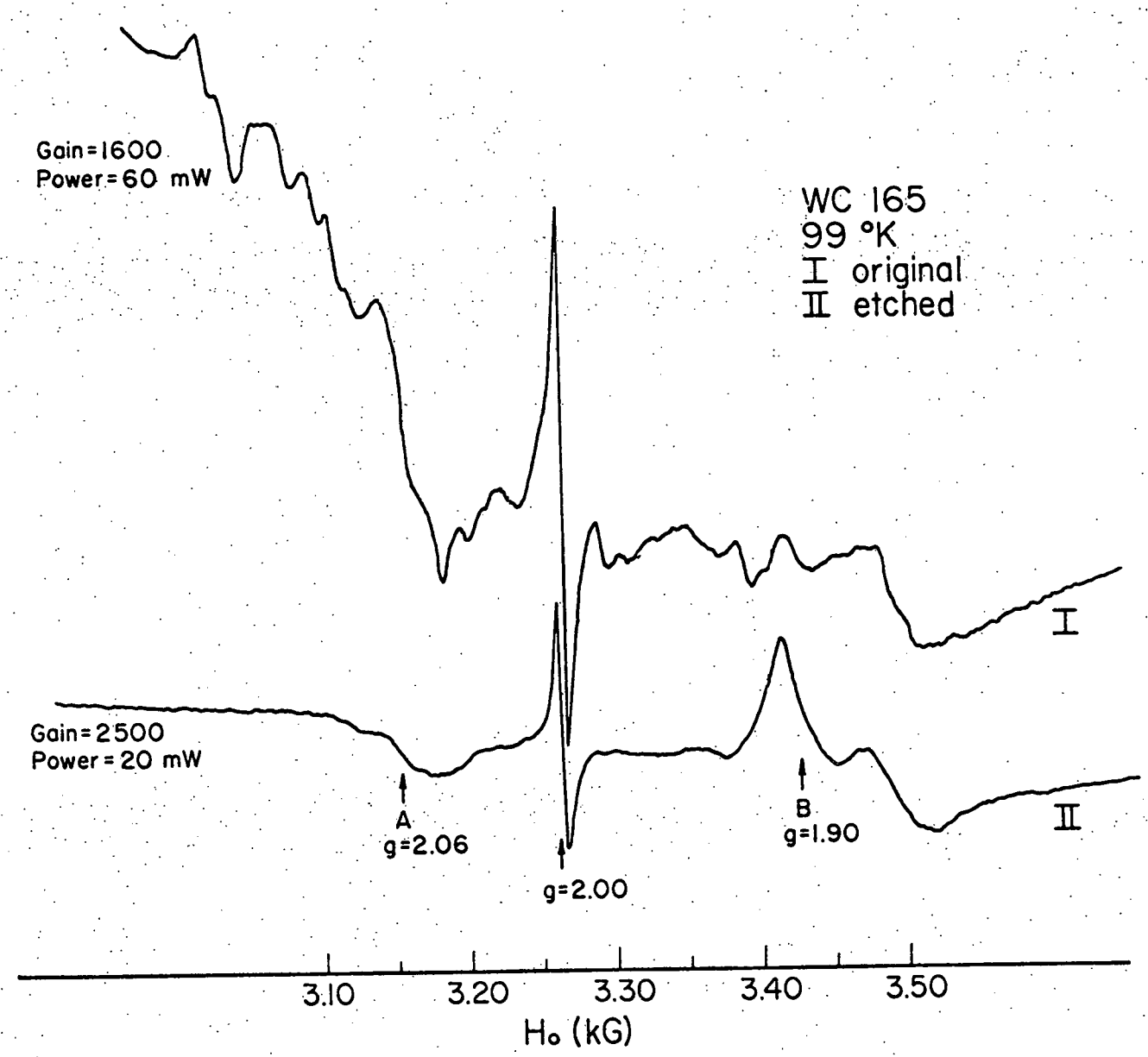

Figure 32. Comparison of ESR signal from original and etched WC 165.

The results of this work, for the TiC_xO_y system, may be interpreted by the two models proposed by Kunz and coworkers.[29] Neither $TiC_{1.0}$ or $TiC_{.64}$ was found to be active in hydrogen oxidation. They did not adsorb measurably different amounts of hydrogen at 0 V in acid or in the gas phase. This result indicates that the dangling d-orbitals found by Jennison, et al.,[34] in the stoichiometric carbide were not useful for chemisorption and did not become more involved with decreasing carbon content. On the other hand, we conclude that the 4s level of titanium was not lowered sufficiently by increased carbon vacancies to make local bonding at the vacancy attractive. The results of Goretzki, et al.,[25] who found hydrogen adsorbing at higher temperatures on the nonstoichiometric TiC can be understood as a consequence of thermal excitation of the Ti to a 4s state, which is lowered by the neighboring carbon vacancy. This excitation energy was not available in our experiments.

We have also found that oxygen in the titanium carbide lattice does not significantly alter the catalytic properties of the host material. On the other hand, theory has predicted that the O^- ion is a highly catalytically reactive species. We therefore conclude that the oxygen in TiC_xO_y is not in the O^- configuration.

We have suggested that it is the carbon vacancies, supported in the surface of the WC powders we have examined, which provide the active sites for the chemisorption of hydrogen. Tungsten metal has one of the strongest bonds to hydrogen of any material. Addition of carbon to this material probably pushes the W 6s up, drawing some portion of the electrons down to fill new levels created by the C-W hybridization. A carbon vacancy allows W to appear locally more like a metal atom--that is, its 6s is lowered and at least partially refilled, although some carbide character will be left to the W orbitals. We also note here that the strength of the carbide-H bond found from PDSC work, although a rough estimate, agrees very well with this idea of a metal-like

site at a vacancy. The lowered 6s increases the reactivity of the W ion to hydrogen. At the same time the bonding to the carbide lattice limits the interaction of the W ion with oxygen and water. We suggest that this special bonding configuration of the W ion is only possible in the symmetry of the hexagonal lattice. The same selectivity of the W ion toward H_2 and O_2 was not found in this experiment for the cubic WC/TiC 70/30 lattice. We have not seen evidence of the O^- ion in the ESCA spectra, although in low but active concentrations this might not be detected.

CHAPTER 4

CONCLUSION

1. The catalytically active surface of tungsten carbide is an inhomogeneous mixture of about 0.4 WO_3 and 0.6 of a tungsten carbide phase. The oxide is probably included during the manufacturing process for these active materials--either from incomplete conversion of pockets of the oxide or from oxygen pick-up and surface oxide nucleation during firing.

2. The surface WC phase is carbon deficient. It may be stabilized in this substoichiometric state by the oxide phase or possibly slight oxygen substitution into it.

3. WC 165 can chemisorb hydrogen. The measured total heat of chemisorption gives a value of 75 kcal/mole for the heat of chemisorption.

4. Carbon vacancies are the active sites for H_2 chemisorption on "WC".

5. The activity of these vacancies can be interpreted as resulting from a local lowering of the W 6s state energy to produce a metal-like electronic environment that includes an s-like orbital to bond with incoming hydrogen. The above value for the heat of chemisorption is consistent with this model.

6. Nonstoichiometric titanium carbide does not chemisorb hydrogen at room temperature. They are also found to be inactive to hydrogen oxidation in acid electrolyte. This result indicates that substitutional oxygen is probably not in the carbide lattice as the O^- ion. The Ti 4s state may not be sufficiently lowered for hydrogen bonding by the introduction of carbon vacancies.

7. ESCA results show that oxygen in the WC_xO_y is not in the O^- electronic state. Thus a model based on $(OH)^-$ covalent bond is not appropriate here.

8. A calibration curve for the determination of the surface compositions of TiC_xO_y from AES data is presented. The curve may be applied to the uncleaned surface if double integration of the differentiated Auger data is used.

9. Titanium oxycarbides with $x + y < 1$ preferentially lose titanium when sputtered. An optimum etching time of 2 min. was found for the conditions of our experiment.

BIBLIOGRAPHY

1. R. B. Levy and M. Boudart, Science, 181, 547 (1973).
2. H. Böhm, Electrochim. Acta, 15, 1273 (1970).
3. D. V. Sokolsky, C. Sh. Palanker, and E. N. Baybatyrov, Electrochim. Acta, 20, 71 (1975).
4. J. H. Sinfelt, Progr. in Solid-State Chem., 10, 55 (1975).
5. S. Trasatti, J. Electroanal. Chem., 39, 163 (1972).
6. J. Heidemeyer, D. Barasel, W. Gellert, and P. Scharner, Coll. Czech. Chem. Comm., 36, 944 (1971).
7. K. Mund, G. Richter, and F. V. Sturm., ibid, 36, 439 (1971).
8. H. Binder, A. Koehling, W. Kuhn, W. Linder, and G. Sandstede, Nature, 224, 1299 (1969).
9. H. Böhm and F. Pohl, Third International Conference on Fuel Cells (Brussels, June, 1969), pp. 183-186.
10. R. A. Radzhiev, V. Sh. Palanker, and D. V. Sokol'skii, Élektrokhimiya, 11, 1340 (1975).
11. V. Sh. Palanker and R. A. Gadzhiev, ibid., 11, 1075 (1975).
12. H. Böhm, J. Power Sources, 1, 177 (1976/77).
13. K. v.Benda, H. Binder, A. Koehling, and G. Sandstede, in: From Electrocatalysis to Fuel Cells, ed., G. Sandstede, Univ. Wash. Press, Seattle, 1972, pp. 87-100.
14. D. Baresel, W. Gellert, W. Sarholz, and G. Schulz-Ekloff, Chem. Ing. Tech., 46, 573 (1974).
15. M. Svata and S. Rudolf, J. Power Sources, 1, 277 (1976/77).
16. V. Sh. Palanker, D. V. Sokolsky, E. A. Mazulevsky, and E. N. Baybatyrov, ibid., 1, 169 (1976/77)
17. R. D. Armstrong, A. F. Douglas, and D. E. Keene, J. Electrochem. Soc., 118, 568 (1971).
18. P. Ross, J. MacDonald, and P. Stonehart, J. Electroanal. Chem., 63, 450 (1975).
19. P. N. Ross and P. Stonehart, J. Catal., 48, 42 (1977).
20. L. H. Bennett, J. R. Cuthill, A. J. McAlister, N. E. Erickson, and R. E. Watson, Science, 184, 463 (1974).
21. R. J. Colton, J-T. J. Huang, and J. W. Rabalais, Chem. Phys. Lett., 34, 337 (1975).
22. H. Bohm and L. Baudendistel, German Patent 2, 106, 599, 1972.
23. J. H. Sinfelt and D. J. C. Yates, Nature, 229, 27 (1971).
24. I. Paseka and J. Balej, Coll. Czech. Chem. Comm., 38, 3600 (1973).
25. H. Goretzki, H. Bittner, and H. Nowotny, Monatsh., 95, 1521 (1964).
26. G. Ertl, in: The Electron Factor in Catalysis on Metals, (NBS Special Publication 475, p. 94, 1977).
27. R. J. H. Voorhoeve, Bull. Am. Ceram. Soc., 21, 281 (1976).
28. T. E. Madey, J. T. Yates, Jr., D. R. Sandstrom, and R. J. H. Voorhoeve, in: Treatise on Solid State Chemistry, ed., N. B. Hanney, Plenum Press, Vol., 6, Chapter 6 (1976).
29. A. B. Kunz, M. P. Guse, and R. J. Blint, in: Electrocatalysis on Non-Metallic Surfaces, (NBS Special Publication 455, p. 53, 1976); M. P. Guse, Ph.D. Thesis (University of Illinois at Urbana-Champaign, 1976, unpublished).

30. J. E. Demuth, Surf. Sci., 65, 369 (1977).
31. G. T. Surratt and A. B. Kunz, Phys. Rev. Lett., 40, 347 (1978).
32. D. L. Klein, Ph.D. Thesis (University of Illinois at Urbana-Champaign, 1978, unpublished).
33. F. S. Stone, J. Solid State Chem., 12, 271 (1975).
34. D. R. Jennison, D. L. Klein, A. B. Kunz, K. M. Hall, and W. S. Williams, in: Electrocatalysis on Non-Metallic Surfaces, (NBS Special Publication 455, p. 87, 1976).
35. V. Ya. Naumenko, Porosh. Metall., 10, 20 (1970).
36. G. D. Bogomolov, S. I. Alyamovskii, G. P. Shveikin, and V. D. Lyubimov, Neorgan. Mater., 6, 1405 (1970).
37. S. I. Alyamovskii, Yu. G. Zainulin, G. P. Shveikin, and P. V. Gel'd, ibid., 9, 596 (1973).
38. W. E. Collins, Anal. Calorimetry, 2, 353 (1970).
39. J. H. Scofield, J. Electron Spectroscopy, 8, 129 (1976).
40. C. L. Eggerding, Ph.D. Thesis, (University of Illinois, Urbana-Champaign, 1976) unpublished.
41. Y. G. Zainulin, S. I. Alaymovsky, and G. P. Shveikin, J. Phys. Chem. Solids, 39, 29 (1968).
42. L. A. Azaroff and M. J. Buerger, The Powder Methods, McGraw-Hill, New York (1958), p. 255.
43. E. K. Storms, The Refractory Carbides, Academic Press, New York (1967), p. 143.
44. J. E. Benson and M. Boudart, J. Catal., 4, 704 (1965); M. A. Bannice, J. E. Benson, and M. Boudart, J. Catal., 16, 348 (1970).
45. J. Bett, M. Kinoshita, K. Routsis, and P. Stonehart, J. Catal., 29, 160 (1973).
46. P. Ross and P. Stonehart, ibid., 39, 298 (1975).
47. J. Haber, J. Stoch, and L. Ungier, J. Solid State Chem., 19, 113 (1976).
48. C. N. Sayer and N. R. Armstrong, Surf. Sci., 77, 301 (1978).
49. K. S. Kim, W. E. Baitinger, J. W. Amy, and N. Winograd, J. Electron Spectroscopy, 5, 351 (1974).
50. D. N. French and D. A. Thomas, in: Anistropy in Single-Crystal Refractory Compounds, Vol. 1, ed., F. W. Vahldiek and S. A. Mersol, Plenum Press, New York (1968), pp. 55-66.
51. C. C. Chang, in: Characterization of Solid Surfaces, ed., P. F. Kane and G. B. Larrabee, Plenum Press, New York (1974), pp. 509-575.
52. T. W. Haas, J. T. Grant, and G. J. Dooley III, J. Appl. Phys., 43, 1 53 (1972).
53. see for examples: W. S. Williams, in Progress in Solid State Chemistry, ed., H. Reiss, (1971), 6,57.
54. J. T. Grant, T. W. Haas, and J. E. Houston, Phys. Lett., 45A, 309 (1973).

VITA

James Roger Bethin

entered the University of Rochester in 1968, and graduated with distinction in 1972 with a B.S. in Physics. He entered the Department of Physics in 1972 at the University of Illinois at Champaign-Urbana and received an M.S. in 1974. He entered the Department of Ceramic Engineering in 1974 and graduated in 1979 with a Ph.D. He was a teaching assistant in the Department of Physics at the University of Illinois in 1972 and was a research assistant in the Department of Physics in 1973. During the course of this work he was a research assistant at the Materials Research Laboratory and the Department of Ceramic Engineering.

He is a member of the American Ceramic Society and the American Physical Society. A list of publications and presentations follows.

"Polarizabilities of Shallow Donors in Silicon," J. Bethin, T. G. Castner, and N. K. Lee, Solid State Communications, 14, 1321-24 (1974).

"Ambipolar Diffusion Contribution to High-Temperature Thermal Conductivity of Titanium Carbide," J. Bethin and W. S. Williams, Journal of the American Ceramic Society, 60, 424-27 (1977). Also presented by first author at the 78th Annual Meeting of the American Ceramic Society, Cincinnati, May 4, 1976.

"Electrocatalysis by Non-Stoichiometric Transition Metal Carbides," J. Bethin and W. S. Williams, presented at the 80th Annual Meeting of the American Ceramic Society, Detroit, May 7, 1978.